Proximity Biosensor Assay for PROTAC Ternary Complex Analysis

Irene Ponzo[‡1], Alice Soldà[‡1], Charlotte Crowe[2], Göran Dahl[3], Stefan Geschwindner*[3], Alessio Ciulli*[2], and Ulrich Rant*[1].

[1] Dynamic Biosensors GmbH Germany, Perchtinger Str. 8-10, 81379, Munich, Germany

[2] Centre for Targeted Protein Degradation, School of Life Sciences, University of Dundee, 1 James Lindsay Place, DD1 5JJ, Dundee, United Kingdom

[3] Mechanistic and Structural Biology, Discovery Sciences, BioPharmaceuticals R&D, AstraZeneca, Gothenburg, Sweden

Targeted protein degradation, PROTAC, molecular glue, ternary complex, kinetics, affinity, avidity, Y-structure, switch-SENSE, CRBN, VHL, Brd, BET.

ABSTRACT: Ternary complexes, consisting of two proteins connected by small molecules like PROTACs or molecular glues pose new challenges for the analysis of molecular interactions, because they depend not only on binary affinities, but are orchestrated by cooperativity and avidity effects. Here, we introduce a proximity binding assay for the simultaneous measurement of binary and ternary interaction kinetics on a biosensor surface. Target proteins and ubiquitin E3 ligase substrate receptors are tethered to mobile swivel arms of a Y-shaped DNA scaffold, which presents them in close proximity to PROTAC analytes flown across the sensor. PROTAC-induced ternary complex formation is measured by fluorescence energy transfer (FRET), while binary interactions are detected by fluorescence quenching. The assay is applied to cereblon (CRBN) and von Hippel-Lindau (VHL) as E3 ligase substrate receptors, a range of compounds including AT1, MZ1, dBETs, and ARV-825 as PROTACs, and the two bromodomains of Brd2, Brd3, Brd4, and BrdT proteins as targets. Automated workflows enable the measurement of 384 real-time sensorgrams in a single run using picomolar sample quantities. Ternary and binary binding kinetics and proximity-mediated binding enhancements are analyzed. Ternary complex stability is shown to arise from a dynamic interplay of associations and dissociations, suggesting that proximity assays can be utilized to identify weak interactions. The insights into proximity-mediated binding kinetics can enable the development of PROTACs and molecular glues with improved properties for targeted protein degradation.

Introduction. Initially described in 2001[1,2], PROTACs (PROteolysis TArgeting Chimeras) have emerged as a powerful therapeutic strategy to selectively degrade proteins via the ubiquitin-proteasome system (UPS). PROTACs are bifunctional small molecules consisting of two protein-binding moieties joined by a linker: one moiety targets a protein of interest (POI), while the other recruits an E3 ubiquitin ligase. By simultaneously engaging both the E3 ligase and the POI, a ternary complex is formed, which enables ubiquitination and subsequent degradation of the POI. Besides PROTACs, molecular glues also induce ternary complex formation, albeit via a distinct molecular mechanism. PROTACs and molecular glues are promising as new drugs and bear advantages compared to other therapeutics, as they can potentially be administered orally and effectively engage intracellular targets[3]. Targeted protein degradation has recently been applied successfully also to receptors on cell surfaces using bispecific antibodies (PROTABs)[4]. The first generation of PROTACs was designed by employing bulky peptide-based E3 ligands, limiting their clinical application[5]. Significant advancements were made in the last decade, leading to the development of PROTACs with improved physical-chemical properties: the most common being recruiters of von Hippel-Lindau (VHL)[6,7] and cereblon (CRBN)[8,9]. These substrate receptors are components of the Cullin-RING E3 ligase (CRL) complexes $CRL2^{VHL}$ and $CRL4^{CRBN}$. In particular, CRBN was identified as the molecular target of the immunomodulatory imide (IMiDs) drugs, thalidomide and derivatives, that are indicated for multiple myeloma[10], and many PROTACs in clinical trials recruit CRBN as the E3 ligase. One of the most studied PROTAC targets is Brd4, belonging to the BET family of proteins. Brd4 contains two bromodomains, BD1 and BD2, known to be involved in the transcriptional regulation of gene expression[11].

The formation of a ternary complex between the target protein, the PROTAC, and the ligase, is key to the PROTAC's mechanism of action and efficient target protein degradation[6,12–16]. Thus, a detailed understanding of how to induce and maintain ternary interactions is essential. *In vitro* biophysical assays are attractive compared to cellular assays and *in-vivo* methods for their well-defined experimental conditions and ease-of-use. The analysis of binding

parameters such as affinity, avidity, and cooperativity can reveal useful details about complex formation and stability, and hence guide drug design. The measurement of association and dissociation kinetics can be especially insightful as it addresses two important questions: how quickly does a PROTAC engage its cognate POI and E3 ligase, and how long does it hold the POI and ligase together to enable enzymatic activity?

Scheme 1 illustrates that the ternary complex forms and decays via intermediate binary complexes. The population of binary and ternary states adjusts according to a dynamic interplay of associations, transient dissociations, and re-associations, until eventually complete dissociation ensues. The observable kinetics and the dynamic equilibria of these processes are governed by the molecular reaction rate constants of association and dissociation, k_{on} and k_{off}, the dissociation constant $K_d=k_{off}/k_{on}$, as well as the concentrations of free reactants and binary complexes. A more detailed reaction scheme, which takes different binary complexes into account, is shown in **Scheme S1** in the Supporting Information.

Scheme 1. Simplified reaction scheme for binary and ternary complex formation and decay between a E3 ligase (A), a PROTAC (B), and a protein-of-interest (C).

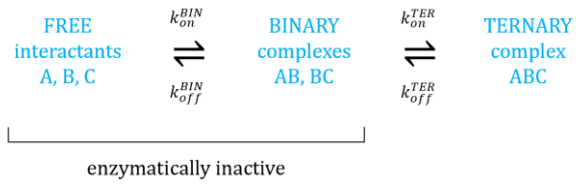

The Y-structure proximity assay measures the formation and decay of the binary complexes via fluorescence quenching (FPS mode), and the formation and decay of ternary complexes via fluorescence energy transfer (FRET mode).

To drive a reaction pathway that effectuates maximal protein degradation, suitable PROTACs or molecular glues with ideal on- and off-rates need to be selected from a (potentially large) pool of candidates. For this purpose, ternary binding must be discriminated from binary binding in a straightforward way[16]. Moreover, the development of high-throughput compatible workflows will facilitate the screening of many compounds. To this end, we devised a chip-based biosensor assay for the investigation of proximity-induced ternary binding, **Figure 1A**. A Y-shaped DNA nanostructure was developed, which tethers two different proteins (a target protein and an E3 ligase substrate receptor) to a sensor at 1:1 stoichiometry and well-defined proximity, see **Figure 1B** and **Scheme 2**. The Y-structure enables the two proteins to swivel freely at the ends of two arms connected at a pivot point and allows them to interact with each other as well as with a third molecule, the bifunctional PROTAC analyte. Binary interactions between the PROTAC and the target or the ligase are followed in real-time by two-color fluorescence detection (quenching), and fluorescence resonance energy transfer (FRET) is used to identify ternary complex formation. The FRET readout directly measures transitions between enzymatically inactive (unary and binary) and potentially active (ternary) states, cf. **Scheme 1**, reaction [2-3]. The observable kinetics do not only depend on molecule-specific rate constants but also reflect the proximity induced between A and C, and hence are structure-specific. The Y-structure creates an environment for avidity, where a bifunctional binder B engages two connected reactants A and C. This assay architecture resembles a situation in which a bifunctional molecule binds to two targets on a cell surface (like an antibody or PROTAB); however, it diverges from a scenario where a PROTAC engages free, unconnected reactants inside a cell. In the latter case, we may compare the proximity induced by the Y-structure in terms of an effective concentration to the solution concentrations of A and C in the cell. The majority (>60%) of proteins in human cells are expressed at copy numbers of 500 to 100,000 molecules per cell[17], which corresponds to nano- to micro-molar concentrations. It will be shown that the proximity induced by the Y-structure is within this physiological range.

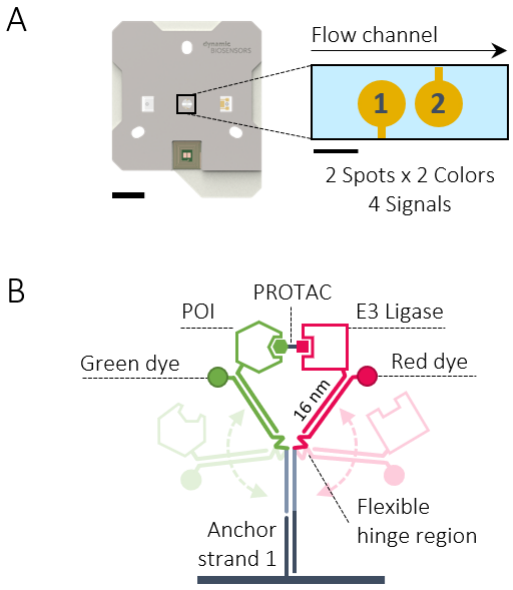

Figure 1. Y-shaped DNA structure for proximity-induced binding assays. (A) Binding kinetics are measured on two gold spots within the microfluidic channel of a heliX® biochip (left scale bar 1 cm; right scale bar 100 µm). Proteins are immobilized on each spot via DNA encoded addressing, utilizing unique anchor strands on the detection spots. (B) The Y-structure is made up of a stem and two swivel arms connected by flexible linkers and consists of four DNA strands. Green and red fluorophores are attached to the distal ends of the swivel arms to detect binary binding via fluorescence quenching (FPS mode) and ternary binding via fluorescence energy transfer (FRET mode). A FRET signal is generated when the arms are closed.

To highlight the advantages of proximity sensing, we compare the Y-structure with conventional assays below

and briefly revisit the meaning of biophysical parameters attainable by different assays. Conventionally, surface plasmon resonance, SPR, has been used as a biophysical technology in PROTAC binding studies (isothermal titration calorimetry and microscale thermophoresis have also been used, but since these methods do not provide kinetic rate constants and calorimetry requires large amounts of sample, they are not discussed further here)[14,18–23]. SPR is a real-time biosensor, where one binding partner is immobilized on a sensor surface, and refractive index changes at the interface are measured upon the accumulation of analyte on the sensor. To measure ternary complex formation induced by bifunctional analytes, sandwich-type assays have been performed, which involve preincubation steps before measuring binding kinetics on the sensor, as shown in **Scheme 2**. First, protein A is immobilized on the surface. Second, the bispecific PROTAC B and protein C are pre-incubated and allowed to form the binary complex BC. Third, the association of $A + BC$ is measured by flowing BC across A on the sensor surface. Fourth, the dissociation of ABC is measured by flowing buffer across the sensor. This procedure has two potential limitations: During the preincubation step, the PROTAC (B) and one of the proteins (C) need to be incubated at concentrations much higher than their dissociation constant. Otherwise, free B, free C, and BC co-exist in the mixture at ill-defined ratios, which impedes an interpretation of the following association and dissociation experiments. In practice, it is often impossible to use concentrations that are high enough when dealing with limited amounts of protein or low-affinity compounds, as solubility issues or increased non-specific interactions with the SPR biosensor matrix may occur. Another difficulty inherent to the sandwich assay is that during the dissociation phase three different types of unbinding events with different kinetics may occur, i.e., $ABC \rightarrow A + BC$ and $ABC \rightarrow AB + C \rightarrow A + B + C$, cf. **Scheme 2** bottom. These three types of dissociations cannot be discriminated by an SPR signal perse, which complicates an interpretation of the observed kinetics. In the Y-structure assay, because both proteins are tethered on the sensor side-by-side, only the PROTAC analyte B needs to be injected during the kinetic experiment, which makes the workflow and data interpretation more straightforward. Furthermore, a refractive index (SPR) measurement does not discriminate between binary or ternary complexes, while the fluorescence readout of the Y-structure assay enables the identification of ternary complexes via FRET.

Different types of binding information are obtained from sandwich and proximity assays. While for both assays, binary and ternary binding parameters may be compared by ratios of their binding constants K_d^{BIN}/K_d^{TER} (or $k_{on}^{TER}/k_{on}^{BIN}$, $k_{off}^{BIN}/k_{off}^{TER}$), the enhancement factors must be interpreted differently, depending on which reactions are probed by the assay. **Equations 1-3** in **Scheme 3** denote the cooperativity factor α, avidity enhancement factor β, and proximity-mediated ternary enhancement factor γ, respectively.

Cooperativity compares the binding constants of a binary interaction in the presence or absence of a third interactant (e.g., for the interaction between A and B: $A + B \rightleftharpoons AB$ vs. $A + BC \rightleftharpoons ABC$). The cooperativity factor α, **Eq. 1**, is obtained from assays where interactants are brought into contact sequentially, i.e., the formation of the ternary complex is measured after a binary complex has been pre-formed, like in sandwich assays[12]. If the first interaction increases the affinity of the second interaction by inducing a higher on-rate and/or a lower off-rate, then $\alpha > 1$ and the cooperativity is positive (conversely, the cooperativity is negative if $\alpha < 1$).

Scheme 2. Y-structure two-color fluorescence assay for ternary interaction analysis (top) versus a conventional SPR-like sandwich assay (bottom).

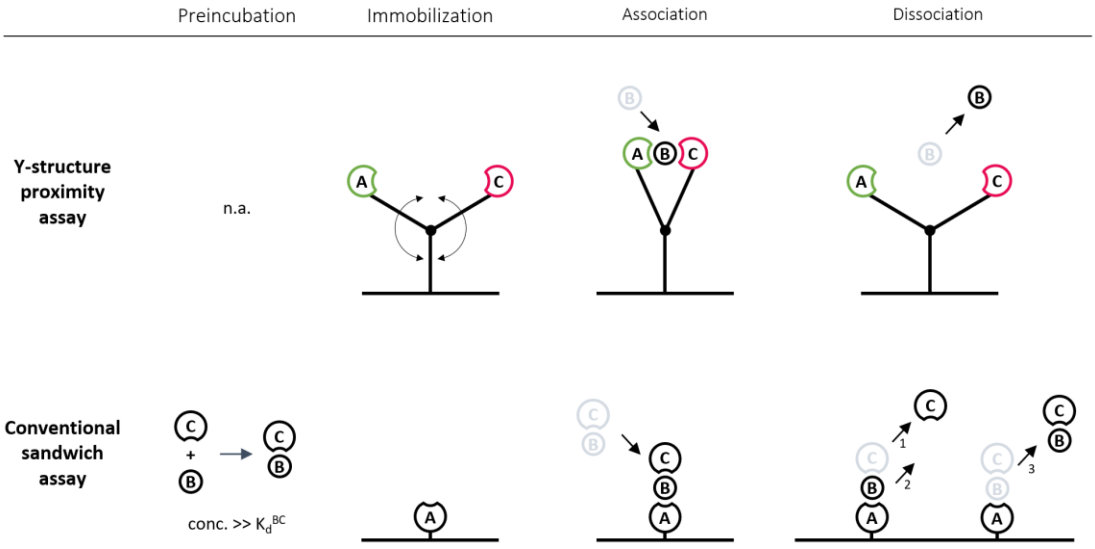

Avidity is a measure of multivalency, which can be defined as the dissociation constant of a multivalent interaction when all interaction sites are associated relative to the completely dissociated form[24], cf. **Eq. 2**. This definition disregards intermediate binary states involved in the assembly and disassembly of the ternary complex. The avidity enhancement factor β compares affinity $K_d's$ of binary interactions to the avidity K_d, which are usually measured in separate experiments.

The proximity-mediated ternary enhancement factor γ is introduced here in the context of the Y-structure assay to describe the increased binding strength of the ternary complex compared to binary complexes. To rationalize it, we need to consider how the binding parameters measured by the Y-structure assay relate to the reaction pathways depicted in **Scheme 1** & **S1**. First, we note that the Y-structure creates an avidity effect, as it establishes a linkage between the E3 ligase and POI through its arms. Because proximity promotes avidity, it is expected that binding parameters measured with a particular Y-structure depend on the proximity effect conferred by its geometry and flexibility. The γ factor is structure-specific, and Y-designs with stronger proximity will stimulate stronger avidity. Second, we must examine which reactions are probed by the two measured fluorescence signals (quenching and FRET), which is depicted in the reaction scheme in **Eq. 3**. Binary interactions are measured by fluorescence quenching and individual sets of binding constants are obtained for $A + B \rightleftharpoons AB$ and $B + C \rightleftharpoons BC$.

Scheme 3. Types of binding information obtained from sandwich and proximity assays.

Type of assay	Reactions probed by assay	Enhancement factor
(1) Cooperativity	$A + B \overset{BIN}{\rightleftharpoons} AB + C \overset{TER}{\rightleftharpoons} ABC$ $B + C \rightleftharpoons A + BC \rightleftharpoons ABC$	$\alpha_{K_d,i} = \frac{K_d^{BIN,i}}{K_d^{TER,i}}$
(2) Avidity	$\underbrace{A + B + C} \overset{AVI}{\rightleftharpoons} \underbrace{ABC}$	$\beta_{K_d,i} = \frac{K_d^{AFFINITY,i}}{K_d^{AVIDITY}}$
(3) Proximity	$\underbrace{A + B + C} \overset{BIN}{\gtrless} \left.\begin{matrix}\underbrace{AB + C} \\ \underbrace{A + BC}\end{matrix}\right\} \overset{TER}{\rightleftharpoons} \underbrace{ABC}$	$\gamma_{K_d,i} = \frac{K_d^{BIN,i}}{K_d^{TER}}$

Horizontal brackets in the reactions of Eq. 2 and Eq. 3 indicate that A and C are connected in avidity and proximity assays. Factors are given for K_d enhancements, but can also be defined for on- and off-rates, e.g., $\gamma_{k\_on} = k_{on}^{TER}/k_{on}^{BIN}$, $\gamma_{k\_off} = k_{off}^{BIN}/k_{off}^{TER}$. All three factors can be calculated with respect to any of the two possible binary complexes leading to a ternary complex, which is reflected by the index $i = AB$ or BC.

Ternary interactions are measured by the FRET signal, which does not discriminate whether binary complexes AB or BC are involved in the assembly or disassembly of the ternary complex, as indicated by the single reaction arrow and curly bracket for the ternary interaction in **Eq. 3**. Being indiscriminate about binary complexes bears the advantage that FRET directly signals if an enzymatically inactive or potentially active state is present. Hence, ternary kinetics observed with the assay can be interpreted within the simple **Scheme 1** rather than considering more complex reaction pathways like **Scheme S1**, which simplifies data analysis.

Using the Y-structure proximity assay, bifunctional analytes can be tested directly with respect to ternary binding. The assay may be applied in the discovery of various candidates for proximity inducing therapeutic modalities[25], such as PROTACs, molecular glues[26], Regulated Induced Proximity Targeting Chimeras (RIPTACs)[27], or transcriptional chemical inducers of proximity (TCIPs)[28]. Here, we demonstrate ternary screens of PROTACs recruiting two different E3 ligase substrate receptors, VHL and CRBN, and different BET proteins as targets.

Results and discussion. A fluorescence biosensor instrument with two-color detection and chips with integrated microfluidic channels, which had been applied previously to investigate various molecular interactions, and in particular multivalent binding[29–34], were used in this study (heliX⁺ instrument and chip, see **Figure 1A**). The chip was used off-the-shelf and featured covalently attached single stranded 48 nucleotides DNA molecules, which serve as "anchors" for further functionalization with DNA-protein conjugates. Four signals, i.e., red and green fluorescence from two sensor spots, were measured simultaneously. The kinetics of association and dissociation of PROTAC analytes to and from ligase and target proteins on the sensor surface were monitored in real-time as changes in the observed fluorescence intensities. Different excitation/emission configurations were used to probe different binding modes: green/green to detect interactions involving the POI immobilized on the 'green arm', red/red to detect interactions involving the E3 ligase immobilized on the 'red arm', and green/red (FRET) to detect the closing of the Y-structure's arms, i.e., ternary complex formation.

The Y-structure for proximity-induced binding. A simple Y-shaped structure was constructed from oligodeoxynucleotides to induce well-defined proximity between target and ligase proteins on the sensor, see **Figure 1B**. The Y-structure is made up of a stem that branches into two swivel arms. The 96 bp stem connects the Y-structure to the surface via a sequence that is complementary to 48 nt anchor-strands, which are fixed on the chip. The sensor is functionalized with fresh Y-structure by DNA hybridization, while used Y-structures are removed from the sensor by denaturing the stem in a high-pH wash, both steps being performed in the instrument automatically.

The swivel arms are 48 bp long and attached to the stem via a flexible hinge region, which enables the arms to rotate by diffusion. The distal ends of the arms may touch or move away from each other, reaching distances up to 40 nm. The arms are each labeled with a red and a green fluorophore, respectively, at their distal ends. The heliX⁺ instrument excites and detects red or green fluorescence separately;

alternatively, it excites the green fluorophore and detects red fluorescence to measure FRET. No significant FRET signal is observed in an open configuration, as the fluorophores are too far apart, but when the arms are closed, a FRET signal is detected. This FRET signal is used to measure the formation of a ternary complex between two proteins attached to the end of the arms, and a third molecule, the PROTAC, see **Figure 1B** and **Figure S1**. Before using the Y-structure for PROTAC measurements, we used interactants with known affinities to characterize its proximity effect. To this end, we extended the arms with overhangs of complementary oligodeoxynucleotides from 4 bp to 15 bp and tested how long (strong) the oligodeoxynucleotides need to become to close the swivel arms by "zipping" them up at their tips. The zipper dissociation constants were characterized in a separate experiment, also using the heliX+ biosensor, and span more than nine orders of magnitude from pM to mM K_d's (**Figure 2**, **Figure S1**). With the obtained affinities, we can plot the open/closed arm configurations versus the zipper K_d in **Figure 2**. For short and weak zippers with less than 6 bp and $K_d's > 10\ \mu M$, the arms remain always open, while for long and strong zippers with more than 12 bp and $K_d's < 1\ nM$, the arms are always closed. When using zippers of intermediate lengths (7 to 11 bp), the arms are partly open and partly closed. This range of affinities with $1\ nM < K_d < 10\ \mu M$ can be considered the Y-structure's dynamic range, as arm configurations dynamically switch between open and closed states. The mid-point, at which 50% of the arms are closed when averaged over time, is observed for a zipper $K_d = 150\ nM$. We may interpret this affinity calibration experiment in terms of an effective concentration: the Y-structure induces a proximity equivalent to an effective concentration of $c_Y = 150\ nM$, because if interactants with a $K_d = 150\ nM$ are attached to the Y-structure's arms, a fraction of 50% is bound. However, we note that the term effective concentration used here is not the same as a solution concentration of molecules diffusing freely in three dimensions, because interactants on a Y-structure are constrained by their attachment to the arms, and the arms' swivel motions. Consequently, different Y-structure designs are expected to feature different effective concentrations, and in fact we observed a hundred-fold difference in effective concentration for an alternative design. To summarize its properties, the Y-structure presented here is suitable to detect ternary interactions with $K_d < 10\ \mu M$ by FRET, while weaker interactions are undetectable. For interactions with $1\ nM < K_d < 10\ \mu M$, the FRET signal intensity scales with the affinity of the interaction and, in principle, the interaction's K_d may be estimated from the calibration curve in **Figure 2**. Interactions with $K_d < 1\ nM$ will generate a maximal FRET intensity that does not depend on the interaction's K_d.

Working principle of the Y-structure assay for PROTAC analysis. To demonstrate the working principle of the Y-structure for PROTAC analysis, we used a well-characterized system composed of VHL-EloB-EloC (VCB) as the E3 ligase substrate receptor and adaptor proteins, the BET bromodomain protein Brd4^{BD2} as the target, and the bifunctional compounds AT1 and MZ1 as PROTACs[12,35]. PROTAC structures are shown in **Scheme S2** in the Supporting Information. To functionalize the Y-structure with ligase and target proteins, proteins were conjugated through NHS ester coupling to DNA strands that were complementary to the sequences of the red and green arms of the Y-structure, using off-the-shelf conjugation kits, and purified by ion exchange chromatography (see Material & Methods in the Supporting Information). The Y-structure was assembled before the sensing experiment by incubating DNA-protein conjugate strands with stem strands and subsequently immobilized on the sensor surface (workflow for sensor regeneration is shown in **Figure S2**).

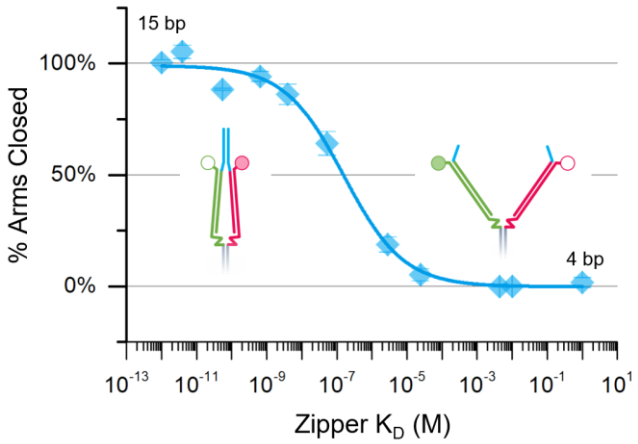

Figure 2. Affinity calibration curve to gauge the Y-structure's proximity effect. Sequence-complementary single stranded oligodeoxynucleotides of variable lengths, ranging from 4 nt to 15 nt, are protruding from the swivel arms ('DNA zippers', shown in blue). The fraction of closed arms inferred from the FRET signal (detection of red dye's fluorescence upon optical excitation of green dye) is plotted versus DNA zipper affinities, which were measured separately (Figure S1). The half-closed midpoint is at 150 nM.

Binary interactions between PROTAC and target, and PROTAC and ligase, were analyzed by functionalizing only one arm with a protein, while the other arm was double stranded but remained unmodified. Binding kinetics were followed in one of two colors: green fluorescence was excited and detected for Brd4^{BD2} target, and alternatively red fluorescence was excited and detected for VCB ligase. In both cases, the Fluorescence Proximity Sensing (FPS) mode was used for detection of PROTAC binding (**Figures 3A** and **3C**). In the FPS detection mode, the fluorescence intensity of a dye attached near a protein is monitored during the association and dissociation of analyte. In the presence of bound analyte, the dye fluorescence is quenched by molecular collisions. This results in a fluorescence decrease during the association phase and a fluorescence increase during the dissociation phase, which is directly proportional to the fraction bound. The kinetics of AT1 binding to Brd4^{BD2}, and AT1 binding to VCB, can both be described well by a 1:1 binding model. Data were fitted globally for all concentrations without the need for mass-transport correction factors using mono-exponential functions $\propto exp\{-(ck_{on} +$

k_{off})t} and $\propto exp\{-k_{off}t\}$ for the association and dissociation phases, respectively. Kinetic rate constants and dissociation constants are depicted in **Figure 3D** and listed in **Table 1**. AT1 has a 10x higher affinity for Brd4^{BD2} ($K_d^{BIN|AT1\cdot Brd4BD2} = 12\,nM$) than for VCB ($K_d^{BIN|AT1\cdot VCB} = 126\,nM$). Notably, this affinity difference is mainly caused by the 20x higher association rate for Brd4^{BD2}, while the durability (half-life) of the interaction is in fact 2x higher for VCB. The $K_d's$ measured here are comparable to literature SPR values (9 nM and 110 nM)[12], although this might be coincidental as SPR values were measured at lower temperatures (12°C vs. 25°C here) and lower flow rates, and, not unexpectedly, feature lower association as well as dissociation rates.

To measure PROTAC-mediated ternary complex formation, both arms of the Y-structure were functionalized with proteins, see **Figure 3B**. Brd4^{BD2} target-conjugate was hybridized to the arm modified with the green dye, and VCB ligase-conjugate was hybridized to the red arm. Fluorescence was excited selectively in green only, while emission was measured in green and red simultaneously. Upon injection of PROTAC analyte, a mirror-like decrease in green fluorescence and a concomitant increase in red fluorescence are detected. The increase in red fluorescence is different from the red signal observed in the binary binding experiments, because neither can red fluorescence be excited directly by the green illumination (cf. the flat line in **Figure 3A**), nor does it exhibit the quenching signature of an FPS-like signal (cf. **Figure 3C**). Therefore, we attribute the red emission to indirect excitation via green-to-red FRET, which results from a closing of the Y-structure as PROTACs interlink target and ligase proteins.

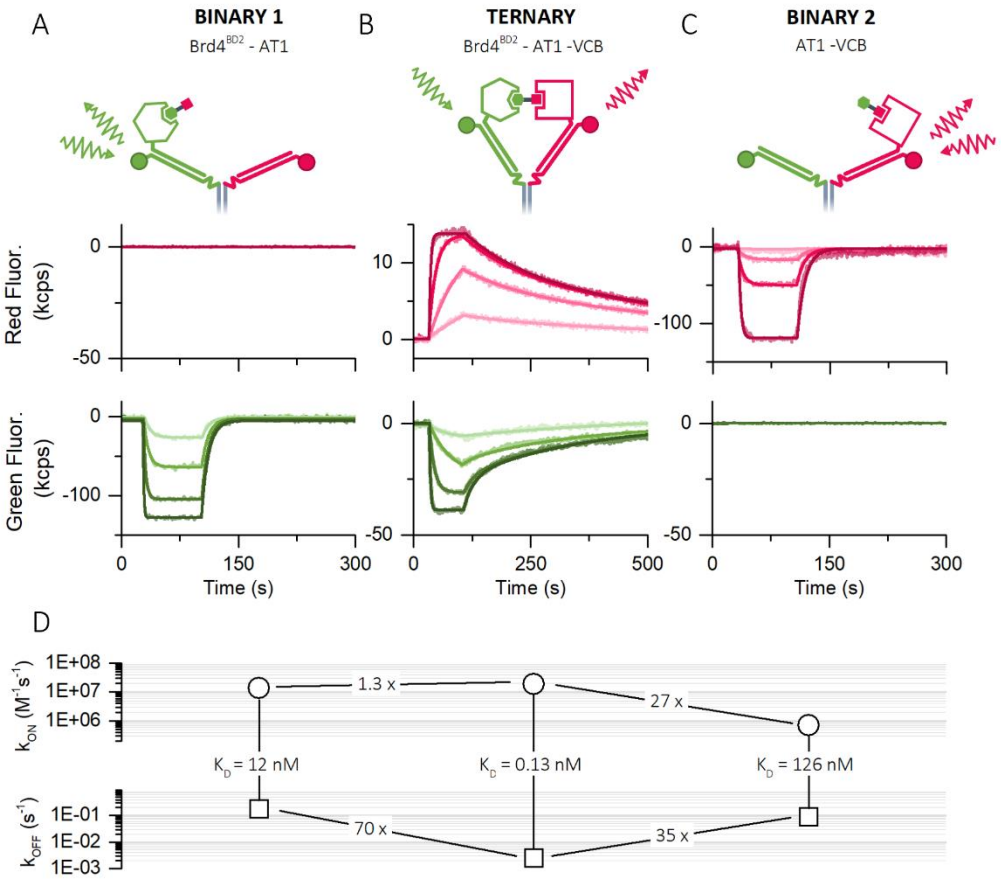

Figure 3. Proximity induced binding assay with a DNA Y-nanostructure for the measurement of binary and ternary binding kinetics of bifunctional small molecules. (A) Binary binding of the PROTAC AT1 to the POI Brd4^{BD2} results in a quenching of green fluorescence (FPS detection). AT1 was injected at concentrations 4 nM, 20 nM, 100 nM, and 500 nM. (B) Ternary binding of AT1 to Brd4^{BD2} and the E3 ligase VCB results in a quenching of green (FPS and FRET) and a simultaneous increase of red fluorescence (FRET). AT1 was injected at concentrations of 0.16 nM, 0.8 nM, 4 nM, 20 nM. (C) Binary binding of AT1 to VCB results in the quenching of red fluorescence (FPS). AT1 was injected at concentrations of 4 nM, 20 nM, 100 nM, 500 nM. (D) Rate scale plot depicting association and dissociation rates (k_{on}, k_{off}), and the dissociation constant (K_d). Binary interactions of AT1 with Brd4^{BD2} and AT1 with VHL are shown on the left and on the right, respectively, while ternary interaction constants are shown in the middle (corresponding to data from A-C)

Table 1. Binding constants of AT1 and MZ1 PROTACs interacting with Brd4^{BD2} and VCB ligase substrate receptor on a Y-structure.

PROTAC	Interaction	POI	Ligase	k_{on} (1E6 $M^{-1}s^{-1}$)	k_{off} (1E-3 s^{-1})	K_d (nM)	$t_{1/2}$ (s)
AT1	Binary	Brd4^{BD2}	-	13.5 ± 2.5	173 ± 35.4	12.8 ± 1.3	4.0
	Binary	-	VCB	0.69 ± 0.12	87.5 ± 26.7	126 ± 20	7.9
	Ternary	Brd4^{BD2}	VCB	18.7 ± 3.00	2.47 ± 0.19	0.13 ± 0.02	280
MZ1	Binary	Brd4^{BD2}	-	11.4 ± 0.7	112 ± 16.3	9.78 ± 0.9	6.2
	Binary	-	VCB	3.61 ± 0.75	66.1 ± 17.1	18.3 ± 0.9	10.5
	Ternary	Brd4^{BD2}	VCB	28.8 ± 6.9	0.80 ± 0.52	0.028 ± 0.017	863

Values shown represent the mean ± SD of at least three independent experiments. $t_{1/2} = \ln 2/k_{off}$ is the dissociation half-life.

We cannot quantify molecular distances accurately, but we estimate from the emission intensities that the green and red dyes reside within 1 to 2 Förster radii of each other when the arms are closed. This corresponds to a distance of roughly 5 to 10 nm, which is reasonable considering the dimensions and the spatial arrangement of the involved molecules. While the red fluorescence increase results from FRET, the green fluorescence decrease is caused by a convolution of two effects, namely, the FPS-like direct quenching by the presence of AT1 and the loss of green emission intensity due to FRET. Hence, the green signal reports binary and ternary binding, whereas the red, FRET-only signal selectively reports the formation and decay of the ternary complex. Ternary binding kinetics in **Figure 3B** can be analyzed by mono-exponential functions as above and the results are summarized in the rate-scale plot in **Figure 3D** and in **Table 1**. Additional analyte concentrations, a comparison of mono- vs. bi-exponential fit models, and duplicates are shown in **Figures S3-S4** in the Supporting Information. The K_d of the ternary complex ($K_d^{TER} = 0.13\ nM$) is much lower than the binary K_d's of the PROTAC for the target ($K_d^{BIN|AT1\cdot Brd4BD2} = 12\ nM, \gamma_{K_d}^{AT1\cdot Brd4BD2} = 92$) or for the ligase ($K_d^{BIN|AT1\cdot VCB} = 126\ nM,\ \gamma_{K_d}^{AT1\cdot VCB} = 969$). The observed kinetics allow us to rationalize the processes involved in the formation and decay of the ternary complex: the rate at which the ternary complex forms is practically identical to the association rate of the fast-binding target Brd4^{BD2}. This suggests that the PROTAC is captured by the target first and passed on without significant delay to the ligase. We can estimate the hand-off time from the slower binary on-rate $k_{on}^{BIN|AT1\cdot VCB}$ and the Y-structure's effective concentration, $\tau \approx 1/ck_{on} \approx 10\ s$; however, this estimate does not take cooperativity into account and thus the actual hand-off time may be shorter or longer. It is important to note that the experiments depicted in **Figure 3B** were carried out with PROTAC concentrations $\leq 20\ nM$, which is low compared to the Y-structure's effective concentration of 150 nM. For higher PROTAC concentrations approaching or exceeding the Y-structure's effective concentration, free PROTAC molecules in solution are expected to compete with target-bound PROTACs on the Y-structure for association to the ligase. This kind of auto-inhibition is frequently encountered during the formation of ternary complexes and commonly referred to as the "hook effect", as it shows a hook-like intensity drop in analyte concentration plots[36]. In fact, we observe the onset of an intensity hook effect and the emergence of biphasic kinetics with increasing PROTAC concentrations (Supporting **Figure S5**), indicating that at high concentrations two molecules of PROTACs may bind to the same Y-structure, one to the target and one to the ligase. Consequently, ternary complex formation is blocked, and the arms remain open.

The dissociation behavior of the PROTAC from the ternary complex is strongly influenced by proximity-mediated avidity. In contrast to the association, where one (the faster) binding partner dominates the behavior, avidity significantly slows the PROTAC's dissociation from both, the target as well as the ligase ($\gamma_{off}^{AT1\cdot Brd4} = k_{off}^{BIN|AT1\cdot Brd4}/k_{off}^{TER|Brd4\cdot AT1\cdot VCB} = 70$, $\gamma_{off}^{AT1\cdot VCB} = 35$), cf. **Figure 3D**. The slowed off-rates can be rationalized by considering the dynamic nature of ternary stability as expressed in Equation (5). A PROTAC may transiently dissociate from one of its partners, but if it re-binds before dissociating completely, the ternary complex forms again and stability is maintained.

To further test this, we assessed another PROTAC binding the same target and ligase, MZ1 (Supporting **Figure S6-S7**). MZ1 features very similar kinetic rate constants like AT1, except for its significantly faster ligase association rate ($k_{on}^{MZ1\cdot VCB} = 5 \times k_{on}^{AT1\cdot VCB}$). Indeed, proximity-mediated effects measured for MZ1 off-rates are significantly higher than for AT1 off-rates. Off-rate enhancement factors are $\gamma_{off}^{MZ1\cdot Brd4} = 140$ versus $\gamma_{off}^{AT1\cdot Brd4} = 70$ for the target, and $\gamma_{off}^{MZ1\cdot VCB} = 83$ versus $\gamma_{off}^{AT1\cdot VCB} = 35$ for the ligase, respectively. This suggests that rebinding by fast on-rates is an important factor for ternary complex stability. In other words, the PROTAC's association propensity impacts the dissociation of the ternary complex, which is an important aspect to be considered in PROTAC design.

Ternary and binary screening of PROTACs binding to Brd4BD2 and CRBN. Next, we performed a screen that simultaneously measures ternary and binary interactions, which is shown in **Figure 4**. The target was Brd4^{BD2}, and the ligase was cereblon-DDB1 (CRBN), because CRBN is of great interest in ongoing drug discovery projects but has been difficult to handle in conventional biophysical assays, exhibiting poor stability and non-specific interactions on SPR

surfaces. A 96 well plate was filled with nineteen compounds (**Scheme S2**) at fixed concentrations of 20 nM: 6 bifunctional molecules known to engage both Brd4^{BD2} and CRBN simultaneously, 9 compounds (bifunctional molecules or monovalent ligands) known to engage either Brd4^{BD2} or CRBN individually, and 2 negative control compounds, which are listed in **Table 2**. Four replicates were performed within the same assay to test for repeatability. 384 real-time binding signals were recorded simultaneously in two colors from two spots during 96 injections. Spot 1 was functionalized with a Y-structure featuring Brd4^{BD2} on the green arm and CRBN on the red arm, and 192 sensorgrams are shown in **Figure 4** (96 red and 96 green signals). Spot 2 was functionalized with a Y-structure with Brd4^{BD2} target only and 2x96 sensorgrams are shown in Supporting **Figure S8**. This configuration enables the simultaneous measurement of ternary complex formation on spot 1 as well as binary kinetics on spot 2 within the same experiment. The biosensor chip was regenerated and freshly functionalized at the end of each row, i.e., every 12 analyte injections. Over the course of 8 regenerations during the measurement of one well plate, 15 pmol of CRBN and 30 pmol of Brd4^{BD2} were consumed. PROTACs that induce the formation of a ternary complex between Brd4^{BD2} and CRBN, i.e., ARV-825 and compounds of the dBET family, can easily be identified in **Figure 4A** by a mirror-like signal response, that is, an increase in the red FRET signal and a concomitant decrease of the green signal. Compounds that only interact with Brd4^{BD2} but not with CRBN, for example MZ1 or MZ2, exhibit a decrease in green fluorescence, but no signal change in red fluorescence. Negative controls do not show any signal change, neither in green nor in red. Simultaneous measurements on spot 2, which is only functionalized with Brd4^{BD2}, validate binary interactions with the target protein and serve as a real-time reference (**Figure S8**).

The screening of the selected compounds yielded six ternary hits: ARV-825, ARV-825(2), dBET1, dBET6, dBET6(2), and dBET260 were identified as PROTACs, which interlink target and ligase. Of note, PROTACs marked with the suffix "(2)" had been obtained from different manufacturers and were exchanged between the authors of this study in a blinded manner. They were consistently identified as hits and their kinetics agree with the compounds without a suffix (see below), too, which corroborates a good reproducibility of the assay. The red signal changes are reproducible from the first to the last row, suggesting a satisfying stability of the functionalized Y-structure over the measurement time of 22h. Binary binding to Brd4^{BD2} was observed for nine small molecules: MZ1, MZ2, MZ4, AT1, and cisMZ1 feature a (+)-JQ1 moiety, which binds to BET proteins, including Brd4^{BD2}. They are PROTACs which recruit VHL, but they do not bind CRBN. The BET bromodomain inhibitor (+)-JQ1 shows a detectable signal in green, demonstrating the high sensitivity of the assay to analyze protein-small molecule binding. Binary binding signals to Brd4^{BD2} are also observed for OTX015, ARV-771, and ZXH-3-26. Pomalidomide (Pom) targets CRBN, but does not generate a signal, as binary binding to the E3 ligase substrate receptor is not read-out in the used assay setup. To confirm that the interaction of Pom with CRBN is detectable, it was measured in a separate assay and a K_d of 499 nM was obtained (**Figure S9**). As expected, VH032 did not give a signal, as it is a monovalent compound that targets VHL alone, and indeed VHL was not present in the assay.

Hit maps, which show ternary versus binary binding signals, are presented in **Figure 4I** and **Figure 4J**. Ternary binding is inferred from the red FRET signal amplitude on spot 1, while binary binding to the target is inferred from the green fluorescence amplitude on spot 2, where only Brd4^{BD2} had been immobilized. Ternary hits (ARV-825 and dBET family) can immediately be identified and discriminated from binary interactions from the relative fluorescence changes plotted in **Figure 4I**. To assess the statistical significance of the identified ternary and binary hits, fluorescence data were analyzed by a two-sample t-test with Welch correction, in which the mean values and standard deviations of red and green signals of each compound (n = 4) were compared with blank injections (n = 16). The resulting p-values are plotted in a hit confidence map in **Figure 4J**. The confidence map is divided into four hit quadrants, namely, ternary and binary, ternary, binary, and no hit, by selecting cut-off values of $p < 0.01$. It shows that ternary and binary binders are correctly identified in the screen and can be discriminated from binary binders and negative controls with satisfying statistical significance.

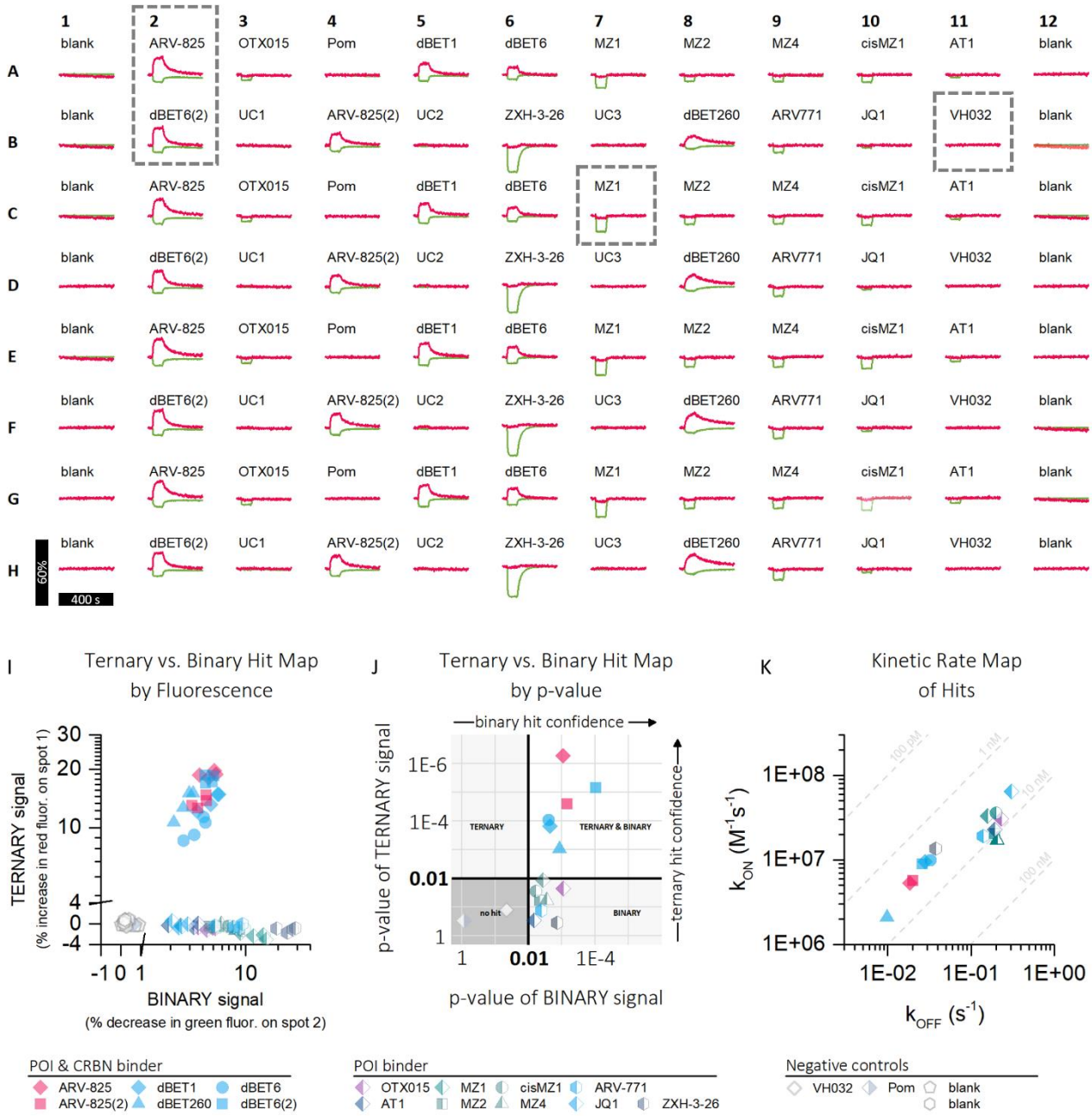

Figure 4. PROTAC screen of 96 samples, measured in two colors on two detection spots. (A-H) Fluorescence sensorgrams of PROTACs interacting with CRBN (red signal) and $Brd4^{BD2}$ (green signal): ARV-825, ARV-825(2), dBET1, dBET6, dBET6(2), and dBET260 PROTACs form ternary complexes between CRBN, PROTAC, and $Brd4^{BD2}$, identifiable by the red FRET signal increase and concomitant quenching of the green signal. Shown are signals from spot 1 with a Y-structure functionalized with $Brd4^{BD2}$ and CRBN. Data from spot 2, functionalized with $Brd4^{BD2}$ only, are shown in Supporting Figure S 7. (I) Ternary vs. binary hit map by fluorescence: percent increase in red fluorescence on spot 1 vs. percent decrease in green fluorescence on spot 2 for all 96 samples. (J) Ternary vs. binary hit map by p-value: p-values of red FRET signals are plotted vs. p-values of green signals (two-sample t-test with Welch correction, n = 4 for each compound, referenced to n = 16 blank traces). (K) Kinetics rate map: mean k_{on} rates versus mean k_{off} rates (n = 4), dashed iso-affinity lines are plotted for K_d = 0.1, 1, 10, and 100 nM. PROTACs forming ternary complexes are depicted as full symbols, binary binders are half full symbols, and negative controls are empty symbols.

Table 2. Kinetic parameters of compounds binding to CRBN and/or Brd4^{BD2} obtained from the screen shown in Figure 3.

PROTAC	Interaction	Target	k_{on} (1E6 $M^{-1}s^{-1}$)	k_{off} (1E-3 s^{-1})	K_d (nM)	$t_{1/2}$ (s)
ARV-825	Ternary	CRBN & Brd4^{BD2}	5.30 ± 1.1	18.6 ± 0.6	3.6 ± 1.0	37.3
ARV-825(2)	Ternary	CRBN & Brd4^{BD2}	5.70 ± 0.4	20.0 ± 1.0	3.5 ± 0.3	34.7
dBET1	Ternary	CRBN & Brd4^{BD2}	8.90 ± 0.7	26.0 ± 0.6	3.0 ± 0.3	26.7
dBET6	Ternary	CRBN & Brd4^{BD2}	9.90 ± 0.5	32.6 ± 1.3	3.3 ± 0.2	21.3
dBET6(2)	Ternary	CRBN & Brd4^{BD2}	9.50 ± 0.7	28.2 ± 1.6	3.0 ± 0.1	24.6
dBET260	Ternary	CRBN & Brd4^{BD2}	2.10 ± 0.1	9.8 ± 0.2	4.6 ± 0.1	70.7
OTX015	Binary	Brd4^{BD2}	30.5 ± 2.6	234 ± 71	7.6 ± 2	2.97
MZ1	Binary	Brd4^{BD2}	32.9 ± 3.7	159 ± 12	4.9 ± 0.4	4.36
MZ2	Binary	Brd4^{BD2}	20.4 ± 2.6	194 ± 17	9.7 ± 1.5	3.57
MZ4	Binary	Brd4^{BD2}	17.1 ± 2.7	207 ± 44	13 ± 5.2	3.35
cisMZ1	Binary	Brd4^{BD2}	35.9 ± 3.7	200 ± 16	5.6 ± 0.9	3.46
AT1	Binary	Brd4^{BD2}	22.8 ± 3.2	193 ± 14	8.7 ± 1.5	3.59
ZXH-3-26	Binary	Brd4^{BD2}	13.6 ± 1.9	37.6 ± 2.0	2.8 ± 0.4	18.4
ARV771	Binary	Brd4^{BD2}	19.1 ± 1.9	141 ± 5.0	7.5 ± 0.7	4.92
JQ1	Binary	Brd4^{BD2}	64.0 ± 22	308 ± 4.8	5.2 ± 1.3	2.25
VH032	N.C.	Brd4^{BD2}	-	-	-	-
Pom	N.C.	Brd4^{BD2}	-	-	-	-
	Binary	$CRBN_{Red}$	0.50 ± 0.02	252 ± 9.5	499 ± 0.01	2.8

Values are means of n = 4 replicates measured at fixed compound concentrations of 20 nM; errors are standard deviations of replicate measurements. The binary interaction of Pom with CRBN was measured separately; t1/2 = ln(2)/koff is the dissociation half-life.

Kinetic hit characterization and validation. Kinetic rate constants k_{on}, k_{off} and K_d values can be analyzed directly from the real-time sensorgrams obtained from the screen. The kinetics of ternary and binary hits can be fitted well with mono-exponential functions, as shown in **Figures S10-S24**. Mean values and standard deviations from four replicates are summarized in **Table 2** and k_{on} and k_{off} rates are plotted in the rate map shown in **Figure 4K**. Relative standard deviations are 6% on average (maximal 21%) for ternary rate constants, and 13% on average (maximal 34%) for binary rate constants, which indicates good repeatability. Of note, the rates of compounds ARV-825 and ARV-825(2) as well as dBET6 and dBET6(2), which were obtained from different manufacturers, superimpose well in the rate map.

The rate map illustrates why it is insightful to measure kinetic binding data instead of inferring steady state K_d values from a titration assay. While most compounds feature very similar K_d values and approximately align along an iso-affinity line in the single-digit nanomolar K_d range, their k_{on} and k_{off} rates are very different. For instance, dBET260 features much slower on- and off-rates than dBET6, yet both have comparable K_d's. Dissimilar binding kinetics may result in different pharmacodynamics, and thus the selection of hits according to their binding kinetics can be valuable for drug development.

For hit validation, we characterized the ternary binders ARV-825 and dBET6, which were designed by the Crews[8] and Bradner[37] laboratories, respectively. The PROTACs are interesting for comparison, as they bind CBRN via the same ligase-binding-moiety, pomalidomide, yet feature different target-binding-moieties, namely OTX015 in the case of ARV-825, and (+)-JQ1 in the case of dBET6. Long linkers connect the moieties for both PROTACs; ARV-825 has a hydrophilic ethylene glycol EG_4 linker, while dBET6 has an alkane C_8 linker.

Sensorgrams with multiple analyte injections are shown in **Figure 5** (ARV-825) and Supporting **Figure S25** (dBET6). Rate constants were analyzed by globally fitting all concentrations using mono-exponential functions and are listed in **Table 3**. Ternary rate constants obtained from the concentration series agree well with screening data that were recorded at a single compound concentration (cf. **Table 2** and **Table 3**), which substantiates the validity of kinetic analyses from screening data.

Binary interactions. For the binary interaction of ARV-825 with Brd4^{BD2} (**Figure 5A**), we obtain a K_d value of 13 nM, which is in the same range as the 28 nM reported from a BROMOscan[8]. Very similar kinetics and K_d values are observed for ARV-825 and dBET6 interacting with Brd4^{BD2}, which seems coincidental, as the PROTACs consist of different target-binding-moieties and linkers. Kinetics of the binary interaction of ARV-825 and CRBN are reported in **Figure 5C**. ARV-825 and dBET6 feature almost identical on-rates (0.5E6 $M^{-1}s^{-1}$) and similar off-rates (79E-3 s^{-1} and 49E-3 s^{-1}), which is not surprising as both PROTACs bind to CRBN via the pomalidomide moiety.

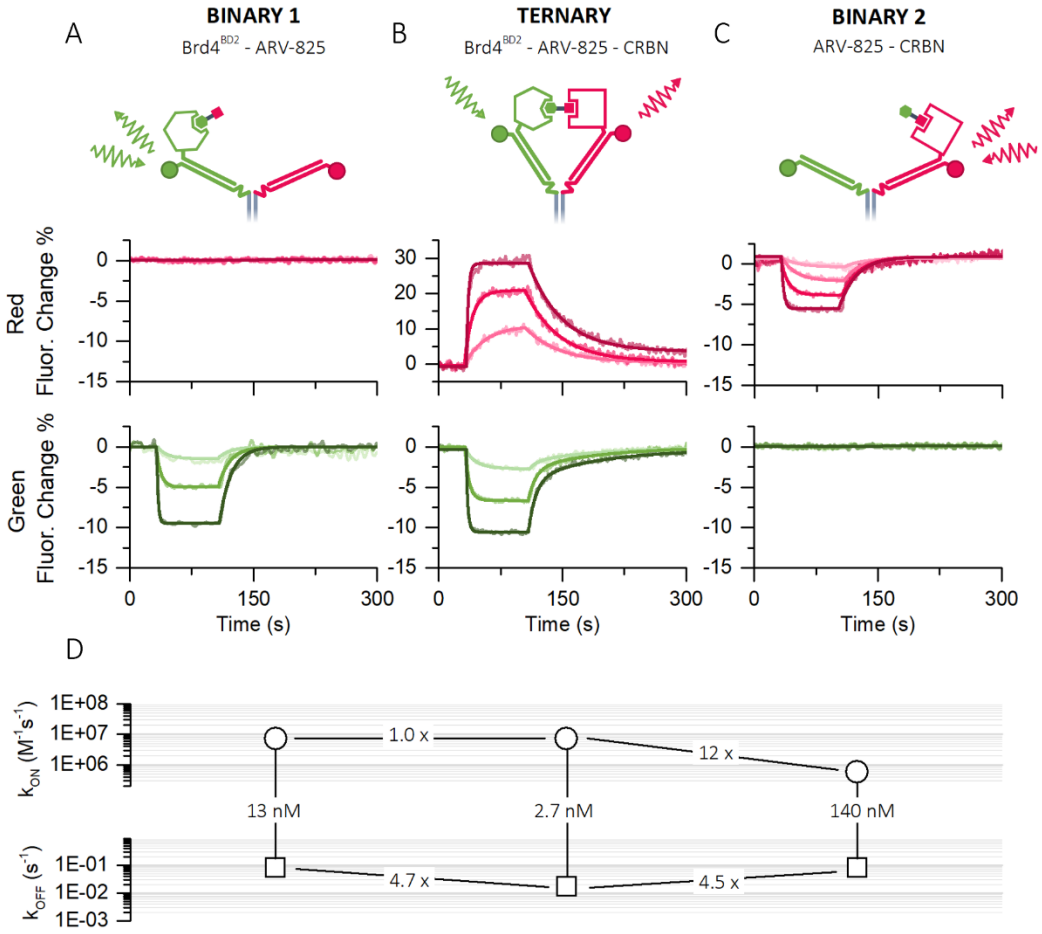

Figure 5. Kinetic characterization of binary *vs* ternary binding of ARV-825 to Brd4^{BD2} and CRBN. (A) Binary binding of ARV-825 to Brd4^{BD2} measured with green excitation. ARV-825 was injected at concentrations of 4 nM, 20 nM, and 100 nM. (B) Ternary binding of ARV-825 to CRBN and Brd4^{BD2}, measured with green excitation. ARV-825 was injected at concentrations of 0.8 nM, 4 nM, and 20 nM. (C) Binary binding of ARV-825 to CRBN measured with red excitation. ARV-825 was injected at concentrations of 4 nM, 20 nM, and 100 nM. (D) Rate scale plot depicting association and dissociation rate constants (k_{on} and k_{off}), and dissociation constants (K_d) of binary (left and right) and ternary (middle) interactions shown in A-C of ARV-825 to Brd4^{BD2}and CRBN.

Table 3. Kinetic rates and dissociation constants of ARV-825 and dBET6 binding to CRBN and Brd4^{BD2}, analyzed from global fit analyses of kinetic measurements at multiple concentrations (Figure 4, Figure S24).

PROTAC	Interaction	POI	Ligase	k_{on} (1E6 $M^{-1}s^{-1}$)	k_{off} (1E-3 s^{-1})	K_d (nM)	$t_{1/2}$ (s)
ARV-825	Binary	Brd4^{BD2}	-	7.10 ± 2.2	83.0 ± 21	12.7 ± 3.7	8.3
	Binary	-	CRBN	0.59 ± 0.17	79.0 ± 19	138 ± 36	8.8
	Ternary	Brd4^{BD2}	CRBN	7.20 ± 2.0	17.8 ± 2.7	2.47 ± 1.10	38.9
dBET6	Binary	Brd4^{BD2}	-	7.25 ± 3.04	91.2 ± 33	12.6 ± 4.9	7.6
	Binary	-	CRBN	0.47 ± 0.35	48.7 ± 9.7	104 ± 126	14.2
	Ternary	Brd4^{BD2}	CRBN	11.3 ± 0.39	31.3 ± 1.2	2.77 ± 1.42	22.1

Values shown represent the mean ± SD of at least three independent experiments. ARV-825: OTX015-EG$_4$-Pom, dBET6: JQ1-C$_8$-Pom

Enhancement factors α^* may be defined to quantify the positive ($\alpha^* > 1$) or negative ($\alpha^* < 1$) effect of non-cognate moieties on the binding behavior of a cognate moieties. For the example of ARV-825, its target-binding-moiety OTX-015, and its target Brd4^{BD2}, α^*'s are calculated as the following ratios: $\alpha^*_{kon} = k_{on}^{ARV825}/k_{on}^{OTX015}$, $\alpha^*_{koff} = k_{off}^{OTX015}/k_{off}^{ARV825}$, $\alpha^*_{Kd} = K_d^{OTX015}/K_d^{ARV825}$ (the ratios resemble cooperativity factors, but the term is not used here to avoid confusion with protein cooperativities as considered in Eq. 1). Analogous expressions can be formulated for other combinations, and the corresponding cooperativity factors are listed in **Table 4**.

The non-cognate parts of ARV-825 as well as dBET6 are found to stabilize binary binding to CRBN. While dissociations are markedly slower ($\alpha^*_{koff} > 3$), no significant effect on the association behavior is observed ($\alpha_{kon} \approx 1$), however. K_d enhancements are dominated by slower dissociations and are positive, too. On the target binding side, the situation is more heterogenous. While ARV-825 and dBET6 dissociate slower than their bare target-binding-moieties ($\alpha^*_{koff} \geq 2.8$), they also associate much slower ($\alpha^*_{kon} \leq 0.2$), which overall weakens affinities ($\alpha^*_{Kd} \approx 0.5$). The results show that it is worthwhile to consider not only the steady state enhancement α^*_{Kd}, but also the kinetic factors α^*_{kon} and α^*_{koff}, because influences of non-cognate on cognate moieties are multifaceted. Effects in a PROTAC's association and dissociation behavior may amplify or counteract each other. It is also interesting to compare dBET6 and AT1, which had been discussed in **Figure 3**, with respect to their target binding properties, because both PROTACs engage Brd4^{BD2} via the same moiety (+)-JQ1. dBET6 and AT1 feature almost identical K_d values of 13 nM, but AT1's on- and off- rates are 2x higher than dBET6's (a statistically significant, yet small difference), which further demonstrates that the behavior of the cognate binding moiety can be influenced by the PROTAC's other domains. The enhancement observed for AT1's (+)-JQ1 target-binding moiety is consistent with the

target-binding moieties of dBET6 (also (+)-JQ1) and ARV-825 (OTX-015): A strongly negative α^*_{kon} dominates a positive α^*_{koff}, which results in an overall negative α^*_{Kd} .

The stability enhancements, which are observed for the ligase as well as the target, might contribute to favorable pharmacodynamics. A positive α^*_{koff} means that a PROTAC, which has bound to any protein, ligase, or target, is less likely to dissociate than the individual bare moieties it comprises. Thus, compared to its bare moieties, the PROTAC has more time to engage the second protein and form a functional ternary complex for protein degradation.

Table 4. Binary binding enhancement factors for PROTACs ARV-825 and dBET6 relative to their constituting moieties OTX015, (+)-JQ1, and Pomalidomide.

PROTAC	Cognate Moiety	Protein	α^*_{kon}	α^*_{koff}	α^*_{Kd}
ARV-825	OTX015	Brd4^{BD2}	0.2	2.8	0.6
	Pom	CRBN	1.2	3.2	3.6
dBET6	(+)-JQ1	Brd4^{BD2}	0.1	3.4	0.4
	Pom	CRBN	0.9	5.2	4.8

Ternary interactions. In **Figure 5B**, we report for the first time the kinetic parameters of ternary complex formation between CRBN, ARV-825 and Brd4^{BD2}. The formation of the ternary complex by ARV-825 corresponds to the binary on-rate of the faster association of the two proteins, i.e., Brd4^{BD2}. This agrees with the observations for dBET6 (Supporting **Figure S25**) as well as AT1 and MZ1 binding to the Brd4/VCB system above. It further supports the interpretation that the PROTAC gets captured by the protein with the higher on-rate first; subsequently, it is handed-off to the protein with the lower association propensity, which is the CRBN ligase. The dissociation kinetics are markedly avid with off-rate proximity-mediated ternary enhancement factors of $\gamma_{koff}^{ARV825 \cdot Brd4BD2} \approx \gamma_{koff}^{ARV825 \cdot CRBN} \approx 5$. However, the proximity factors are significantly lower than for MZ1, which could be due to MZ1's pronounced cooperativity (22 for K_d and 8 for k_{on})[12]or because high binary on-rates drive strong avidity, as the on-rate of MZ1 (3.6E6 $M^{-1}s^{-1}$) is higher than the on-rates of ARV-825/dBET6 for CRBN (~0.6E6 $M^{-1}s^{-1}$).

Analysis of ternary binding to different BET proteins. An important aspect to be considered for the clinical exploitation of PROTACs is their selectivity for BET proteins of different families, and potentially also for different bromodomains on the same BET protein. Because the bromodomains of different BET proteins are highly similar within the ligand binding sites, many BET inhibitors (and also BET PROTACs constructed from them) have been found to be pan-BET binders and do not substantially discriminate between the different BET proteins[38–42]. On the other hand, it has been found in numerous studies that the mechanism of action of the PROTAC via the ternary complex adds an extra layer of selectivity for degradation activity over the selectivity of binary binding[12,19,35,43,44]. To demonstrate the applicability of the introduced method for assessing the binding selectivity of PROTACs for different target proteins, we investigated the ternary binding of ARV-825 to CRBN and to the two different bromodomains BD1 and BD2 of four different BET proteins: Brd2, Brd3, Brd4, and BrdT.

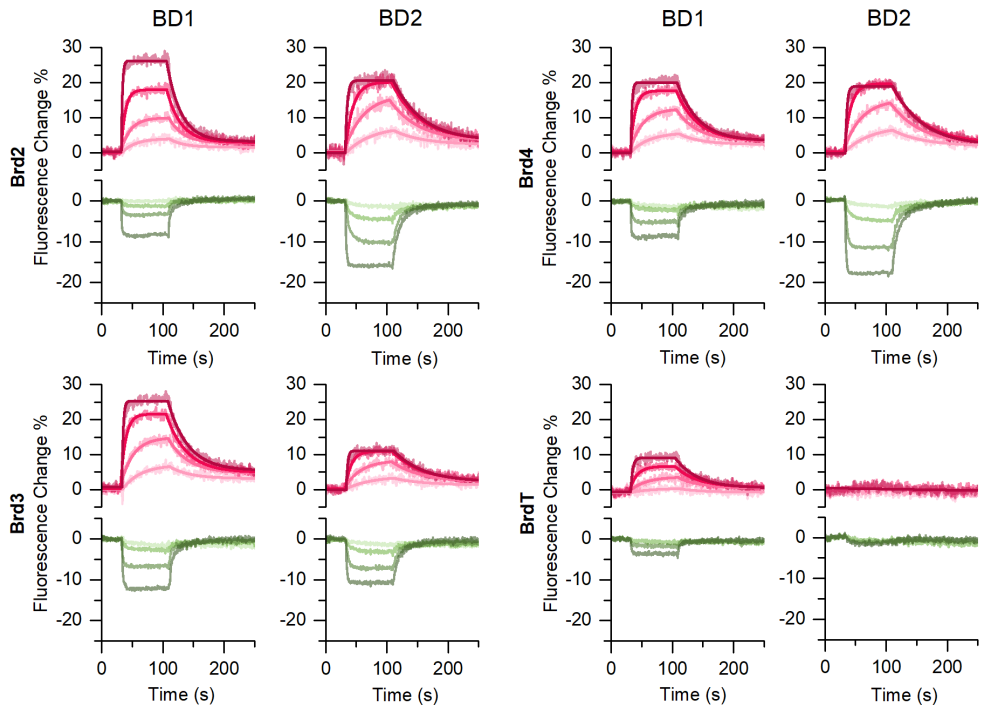

Figure 6. Ternary complex formation sensorgrams of ARV-825 binding to CRBN and bromodomains BD1 and BD2 of different BET proteins: Brd2, Brd3, Brd4 and BrdT. Individual bromodomains (BD1 or BD2) of each BET protein (Brd2, Brd3, Brd4 and BrdT) were immobilized on the Y-structure's green arm and CRBN was immobilized on the red arm. ARV-825 analyte was injected at concentrations of 0.8 nM, 4.0 nM, 20 nM, 100 nM. Fluorescence was excited in green and detected in green (FPS and FRET) and red (FRET).

Table 5. Ternary interaction of ARV-825 with CRBN and different BET proteins.

BET protein	k_{on} (1E6 $M^{-1}s^{-1}$)	k_{off} (1E-2 s^{-1})	K_d (nM)	$t_{1/2}$ (s)
Brd2^{BD1}	8.11 ± 2.50	3.32 ± 0.02	4.52 ± 1.41	20.9
Brd2^{BD2}	4.45 ± 1.01	2.59 ± 0.21	5.82 ± 0.89	26.7
Brd3^{BD1}	6.80 ± 1.62	2.78 ± 0.18	4.08 ± 0.75	24.9
Brd3^{BD2}	5.58 ± 0.92	2.49 ± 0.43	4.46 ± 1.55	27.8
Brd4^{BD1}	8.09 ± 0.12	2.83 ± 0.19	3.50 ± 0.29	24.5
Brd4^{BD2}	5.99 ± 0.26	2.52 ± 0.29	4.20 ± 0.67	27.5
BrdT^{BD1}	4.91 ± 1.03	2.87 ± 0.31	5.84 ± 1.38	24.1
BrdT^{BD2}	n.d.	n.d.	n.d.	n.d.

Bromodomains BD1 and BD2 of the BET proteins Brd2, Brd3, Brd4 and BrdT were tested. Kinetic rate constants were analyzed from red FRET signals, which indicate ternary binding. n.d. - not detected. Values shown represent the mean ± SD of at least three independent experiments.

Sensorgrams are shown in **Figure 6** and ternary and binary interactions are observed across the Brd family of proteins, except for BD2 of BrdT. Again, red signals denote ternary binding via FRET, while green signals are a convolution of binary and ternary interactions via FPS and FRET. Differences in signal amplitudes between different bromodomains and Brd's may be caused by different spatial distances between donor and acceptor dyes for different ternary complexes (different FRET efficiencies), and different dye quenching by different bromodomains (FPS).

Very similar ternary interactions are observed for Brd2, Brd3, and Brd4 for the tested ARV-825 concentration range from 0.8 nM to 100 nM. In fact, the analyzed binding rate constants (cf. **Table 5**) are virtually indistinguishable within the margin of error, indicating that ARV-825 does not discriminate between any of these BET proteins. Slight differences for the two bromodomains can be identified at close inspection: In the presence of CRBN, ARV-825 associates slightly faster to BD1, while it dissociates slightly slower from BD2. This minor tendency is not observed in the absence of CRBN, though (binary interactions of ARV-825 and Brd without CRBN were measured simultaneously on the sensor's second detection spot as before and results are shown in Supporting **Figure S26** and **Table S4**). Our

results agree with other observations in that ARV-825 is a promiscuous, pan-BET binder[42], which does not discriminate between Brd2, Brd3, and Brd4. Yet notably, it does not interact with BD2 of BrdT up to the highest tested concentration of 100 nM.

Conclusions. The Y-nanostructure is an efficient and simple means to enable the analysis of ternary interactions by induced proximity. It keeps two of three interactants tethered to the surface, so that kinetic assays may be run straightforwardly by flowing a single analyte across the surface. This resolves the issue of indistinguishable multi-step reactions in the measurement of kinetics using conventional sandwich-type approaches, and it dramatically reduces sample consumption when screening many compounds. The structural simplicity of the Y-structure allows for simple self-assembly in a one-pot reaction and efficient immobilization on a DNA-modified biosensor surface. The parallel measurement of fluorescence quenching and FRET in two colors on two sensor spots enables the simultaneous analysis and dissection of binary and ternary binding modes. The FRET signal, which arises from a closing of the Y-structure's arms, provides a robust readout, and unequivocally indicates the formation of a ternary complex. It does not discriminate which binary complex is involved in the formation or decay of the ternary complex (AB or BC, cf. Eq. 3) and hence purely reports if the system is broken apart (any binary or unary complex) or bound altogether (ternary complex).

Ternary complex formation is a prerequisite for the mode of action of protein degraders, and the introduced chip-based method can be useful in the discovery of PROTACs and molecular glues to identify and rank ternary binders from a compound pool. It has been shown that ternary complex stability, not just binary affinity, can be important for achieving efficient degradation[16,35,45] and that ternary complex half-life can correlate with degradation efficiency and initial rate[12,14]. With the proximity assay, PROTACs with different half-lives could be readily discriminated in a screen, although they featured almost identical K_d-values. Moreover, non-cognate moieties were found to generally enhance the binding stability, but not the association propensity, of cognate moieties (parental warheads) in the investigated PROTACs.

The prediction of degradation efficiencies for *in-vitro* cell-based assays or even drug efficacy *in-vivo* from binding data is desirable but not straightforward. The assays described here probe ternary binding, which is a necessary, but not sufficient condition for enzymatic activity. For example, dBET6 is reported to be a better degrader than dBET1[37,46], because of better intracellular permeability and stability[37], yet the binding parameters analyzed here are similar. Moreover, degradation concentrations from *in-vitro* cellular assays must be compared carefully, because DC_{50} values depend on the type of cell, type of functional assay, target version, and the incubation time[13,47]. Nonetheless, the literature agrees for degradation of Brd4 via CRBN that ARV-825 is more potent than dBET6, and for degradation via VCB that MZ1 is more potent (yet less Brd4-selective) than AT1, albeit reported DC_{50} values vary (ARV-825: <1 nM for Burkitt's lymphoma cells[8], 0.6 nM for 22RV1[48], 1 nM for NAMALWA[49], 1 nM for CA46[49], 5 nM for Jurkat[50] and Molt[50], 26 nM for 6 T-CEM[50]; dBET6: app. 50 nM for HEK293T[43], app. 100 nM for 661W[51], <500 nM for glioblastoma[52]; MZ1: app. 3 nM for HeLa[53], 23 nM (K_m) for Flp293T[47]; AT1: 10 – 100 nM for HeLa[35]). The same trend is observed for the ternary complex half-life, but not the affinity, in the proximity assay. For both ligases, the PROTACs with the longer half-lives are also the better degraders ($t_{1/2}^{ARV-825} = 2 \times t_{1/2}^{dBET6}$, $t_{1/2}^{MZ1} = 3 \times t_{1/2}^{AT1}$), while almost identical K_d's were measured for ARV-825 and dBET6, which corroborates previous findings[12] that binding kinetics are better than affinity values in suggesting degradation success.

The Y-structure acts as a flexible linker between the POI and the E3 ligase and hence creates a configuration for avidity, where a solute bispecific analyte encounters two binding sites tethered to a surface. The proximity generated between POI and ligase is a crucial parameter, which may be interpreted in terms of an effective concentration c_{eff} (effective molarity). It reflects the ability of the two proteins to collide and interact with each other and the PROTAC. The effective concentration is influenced by the conformation and flexibility of the Y-structure, and how the proteins are attached to it, which defines the range of motion accessible to the proteins. To gauge the Y-structure's effective concentration, we used affinity-calibrated DNA zippers and obtained a value of 150 nM. This value differs drastically from oversimplified geometrical estimates; for instance, if one assumes that reactants are confined to a volume whose dimensions are given by the lengths of the Y-structure's arms, c_{eff} is estimated to be roughly 100 µM, i.e., three-orders-of-magnitude higher. Obviously, the restrictedness of the swivel motion and probably also electrostatic self-repulsion of the DNA arms affect ternary complex formation, and the term *effective* concentration underlines that the mobility of reactants tethered to the Y-structure deviates from three-dimensional diffusion in free solution. Its value depends on the Y-structure design and the characteristics (and coupling) of the attached proteins, and while it may be difficult to quantify c_{eff} for a given set of proteins under investigation, its utility lies more in its conceptual value when compared to the *in-vivo* environment: If the proximity effect mediated by the Y-structure mimics the abundance of proteins within a cell, the binding rates and constants measured with a Y-structure assay are expected to resemble the binding parameters encountered *in-vivo*. In this condition of 'matched proximity', c_{eff} is comparable to the concentrations of target proteins in the lumen of a cell, or comparable to the surface concentrations of target proteins on the cell membrane. If c_{eff} is considerably greater than *in-vivo* target protein concentrations, we refer to 'hyper proximity', and the binding parameters measured with the Y-structure are expected to deviate from the cellular situation. Hyper proximity induces pronounced rebinding ($\propto c_{eff} \cdot k_{on}$), which delays the dissociation process and lowers the apparent K_d. For the two ligases investigated here, the proximity effect is more pronounced for the smaller VCB ligase (41 kDa), for which DC_{50} values (e.g. 3 nM for MZ1) differ 100-fold from

apparent ternary K_d's (0.03 nM). By contrast, in case of the larger CRBN ligase (180 kDa) DC_{50} values and ternary K_d's are similar (e.g. $DC_{50} \approx K_d = 3\,nM$ for ARV-825). We assume that the motion of the smaller VCB ligase on the Y-structure is less restricted, which promotes a hyper proximity effect, while for CRBN the proximity effect is better matched to the cellular situation, and hence the similar magnitude of DC_{50} and K_d values.

While hyper proximity may be considered an artefact in the analysis of high-affinity PROTACs like MZ1, it can be desirable and open new strategies for the discovery of low-affinity compounds. Compounds from a fragment library or molecular glues, which interact only weakly with target proteins, often cannot be identified with conventional screening methods, as at least two of three ternary interactants would need to be incubated at impractically high concentrations. A strong proximity effect can induce ternary complex formation already for weak interactants and enable the identification of otherwise undetectable drug candidates.

We anticipate that the multivariate information on ternary and binary complex provided by the Y-structure assay, in conjunction with the ability to screen many compounds at low sample consumption, will aid the characterization and optimization of future PROTACs, molecular glues, and other bispecific proximity-inducing matchmakers.

ASSOCIATED CONTENT

Supporting Information. Additional reaction pathways, materials and methods, chemical structures, workflow schematics, sensorgrams, chromatograms. This material is available free of charge via the Internet at http://pubs.acs.org.

AUTHOR INFORMATION

Corresponding Author

Ulrich Rant – Dynamic Biosensors Gmbh, Perchtinger Str. 8-10, 81379, Munich Germany; orcid.org/0000-0002-6100-828X; Email: ulrich.rant@dynamic-biosensors.com
Alessio Ciulli – Centre for Targeted Protein Degradation, School of Life Sciences, University of Dundee, 1 James Lindsay Place, DD1 5JJ, Dundee, United Kingdom; orcid.org/0000-0002-8654-1670;
Email: a.ciulli@dundee.ac.uk
Stefan Geschwindner – Mechanistic and Structural Biology, Discovery Sciences, BioPharmaceuticals R&D, AstraZeneca, Gothenburg, Sweden; orcid.org/0000-0002-2154-8345;
Email: stefan.geschwindner@astrazeneca.com

Author Contributions

The manuscript was written and edited through contributions from all authors. I.P., A.S. carried out biosensor experiments, C.C., G.D. prepared/provided proteins and small molecules. Data were analyzed by I.P., A.S., U.R., and reviewed and discussed by all authors. U.R., A.S., A.C., S.G. planned and supervised the project. All authors have given approval to the final version of the manuscript. ‡These authors contributed equally.

Funding Sources

Notes (Competing interests)

I. P., A. S. and U. R. are employed at Dynamic Biosensors which commercializes the heliX® biosensors used in this study. The Ciulli laboratory receives or has received sponsored research support from Almirall, Amgen, Amphista Therapeutics, Boehringer Ingelheim, Eisai, Merck KGaA, Nurix Therapeutics, Ono Pharmaceutical and Tocris-Biotechne. A.C. is a scientific founder, shareholder, and advisor of Amphista Therapeutics, a company that is developing targeted protein degradation therapeutic platforms. The remaining author(s) declare no competing interests.

ACKNOWLEDGMENT

I.P. received funding from the European Union Horizon 2020 Research and Innovation Programme under the Marie Sklodowska-Curie grant agreement No 765266 (LightDyNAmics). C.C. is funded by a PhD studentship from the UK Medical Research Council (MRC) under the Industrial Cooperative Awards in Science & Technology (iCASE) doctoral training programme (MR/R015791/1).

ABBREVIATIONS

TPD targeted protein degradation; PROTAC proteolysis targeting chimera; POI protein of interest; CRBN Cereblon-DDB1; VHL von Hippel-Lindau; FRET fluorescence energy transfer; FPS fluorescence proximity sensing;.

REFERENCES

(1) Sakamoto, K. M.; Kim, K. B.; Kumagai, A.; Mercurio, F.; Crews, C. M.; Deshaies, R. J. Protacs: Chimeric Molecules That Target Proteins to the Skp1–Cullin–F Box Complex for Ubiquitination and Degradation. *Proc. Natl. Acad. Sci. U.S.A.* **2001**, *98* (15), 8554–8559. https://doi.org/10.1073/pnas.141230798.

(2) Békés, M.; Langley, D. R.; Crews, C. M. PROTAC Targeted Protein Degraders: The Past Is Prologue. *Nat Rev Drug Discov* **2022**, *21* (3), 181–200. https://doi.org/10.1038/s41573-021-00371-6.

(3) O'Brien Laramy, M. N.; Luthra, S.; Brown, M. F.; Bartlett, D. W. Delivering on the Promise of Protein Degraders. *Nat Rev Drug Discov* **2023**, *22* (5), 410–427. https://doi.org/10.1038/s41573-023-00652-2.

(4) Marei, H.; Tsai, W.-T. K.; Kee, Y.-S.; Ruiz, K.; He, J.; Cox, C.; Sun, T.; Penikalapati, S.; Dwivedi, P.; Choi, M.; Kan, D.; Saenz-Lopez, P.; Dorighi, K.; Zhang, P.; Kschonsak, Y. T.; Kljavin, N.; Amin, D.; Kim, I.; Mancini, A. G.; Nguyen, T.; Wang, C.; Janezic, E.; Doan, A.; Mai, E.; Xi, H.; Gu, C.; Heinlein, M.; Biehs, B.; Wu, J.; Lehoux, I.; Harris, S.; Comps-Agrar, L.; Seshasayee, D.; De Sauvage, F. J.; Grimmer, M.; Li, J.; Agard, N. J.; De Sousa E Melo, F. Antibody Targeting of E3 Ubiquitin Ligases for Receptor Degradation. *Nature* **2022**, *610* (7930), 182–189. https://doi.org/10.1038/s41586-022-05235-6.

(5) Pettersson, M.; Crews, C. M. PROteolysis TArgeting Chimeras (PROTACs) — Past, Present and Future. *Drug Discovery Today: Technologies* **2019**, *31*, 15–27. https://doi.org/10.1016/j.ddtec.2019.01.002.

(6) Bondeson, D. P.; Mares, A.; Smith, I. E. D.; Ko, E.; Campos, S.; Miah, A. H.; Mulholland, K. E.; Routly, N.; Buckley, D. L.; Gustafson, J. L.; Zinn, N.; Grandi, P.; Shimamura, S.; Bergamini, G.; Faelth-Savitski, M.; Bantscheff, M.; Cox, C.; Gordon, D. A.; Willard, R. R.; Flanagan, J. J.; Casillas, L. N.; Votta, B. J.; Den Besten, W.; Famm, K.; Kruidenier, L.; Carter, P. S.; Harling, J. D.; Churcher, I.; Crews, C. M. Catalytic in Vivo Protein Knockdown by Small-Molecule PROTACs. *Nat Chem Biol* **2015**, *11* (8), 611–617. https://doi.org/10.1038/nchembio.1858.

(7) Diehl, C. J.; Ciulli, A. Discovery of Small Molecule Ligands for the von Hippel-Lindau (VHL) E3 Ligase and Their Use as Inhibitors and PROTAC Degraders. *Chem Soc Rev* **2022**, *51* (19), 8216–8257. https://doi.org/10.1039/d2cs00387b.

(8) Lu, J.; Qian, Y.; Altieri, M.; Dong, H.; Wang, J.; Raina, K.; Hines, J.; Winkler, J. D.; Crew, A. P.; Coleman, K.; Crews, C. M. Hijacking the E3 Ubiquitin Ligase Cereblon to Efficiently Target BRD4. *Chemistry & Biology* **2015**, *22* (6), 755–763. https://doi.org/10.1016/j.chembiol.2015.05.009.

(9) Yamamoto, J.; Ito, T.; Yamaguchi, Y.; Handa, H. Discovery of CRBN as a Target of Thalidomide: A Breakthrough for Progress in the Development of Protein Degraders. *Chem Soc Rev* **2022**, *51* (15), 6234–6250. https://doi.org/10.1039/d2cs00116k.

(10) Ito, T.; Ando, H.; Suzuki, T.; Ogura, T.; Hotta, K.; Imamura, Y.; Yamaguchi, Y.; Handa, H. Identification of a Primary Target of Thalidomide Teratogenicity. *Science* **2010**, *327* (5971), 1345–1350. https://doi.org/10.1126/science.1177319.

(11) Belkina, A. C.; Denis, G. V. BET Domain Co-Regulators in Obesity, Inflammation and Cancer. *Nat Rev Cancer* **2012**, *12* (7), 465–477. https://doi.org/10.1038/nrc3256.

(12) Roy, M. J.; Winkler, S.; Hughes, S. J.; Whitworth, C.; Galant, M.; Farnaby, W.; Rumpel, K.; Ciulli, A. SPR-Measured Dissociation Kinetics of PROTAC Ternary Complexes Influence Target Degradation Rate. *ACS Chem. Biol.* **2019**, *14* (3), 361–368. https://doi.org/10.1021/acschembio.9b00092.

(13) Riching, K. M.; Mahan, S.; Corona, C. R.; McDougall, M.; Vasta, J. D.; Robers, M. B.; Urh, M.; Daniels, D. L. Quantitative Live-Cell Kinetic Degradation and Mechanistic Profiling of PROTAC Mode of Action. *ACS Chem. Biol.* **2018**, *13* (9), 2758–2770. https://doi.org/10.1021/acschembio.8b00692.

(14) Dragovich, P. S.; Pillow, T. H.; Blake, R. A.; Sadowsky, J. D.; Adaligil, E.; Adhikari, P.; Chen, J.; Corr, N.; Dela Cruz-Chuh, J.; Del Rosario, G.; Fullerton, A.; Hartman, S. J.; Jiang, F.; Kaufman, S.; Kleinheinz, T.; Kozak, K. R.; Liu, L.; Lu, Y.; Mulvihill, M. M.; Murray, J. M.; O'Donohue, A.; Rowntree, R. K.; Sawyer, W. S.; Staben, L. R.; Wai, J.; Wang, J.; Wei, B.; Wei, W.; Xu, Z.; Yao, H.; Yu, S.-F.; Zhang, D.; Zhang, H.; Zhang, S.; Zhao, Y.; Zhou, H.; Zhu, X. Antibody-Mediated Delivery of Chimeric BRD4 Degraders. Part 2: Improvement of In Vitro Antiproliferation Activity and In Vivo Antitumor Efficacy. *J. Med. Chem.* **2021**, *64* (5), 2576–2607. https://doi.org/10.1021/acs.jmedchem.0c01846.

(15) Riching, K. M.; Vasta, J. D.; Hughes, S. J.; Zoppi, V.; Maniaci, C.; Testa, A.; Urh, M.; Ciulli, A.; Daniels, D. L. Translating PROTAC Chemical Series Optimization into Functional Outcomes Underlying BRD7 and BRD9 Protein Degradation. *Current Research in Chemical Biology* **2021**, *1*, 100009. https://doi.org/10.1016/j.crchbi.2021.100009.

(16) Bondeson, D. P.; Smith, B. E.; Burslem, G. M.; Buhimschi, A. D.; Hines, J.; Jaime-Figueroa, S.; Wang, J.; Hamman, B. D.; Ishchenko, A.; Crews, C. M. Lessons in PROTAC Design from Selective Degradation with a Promiscuous Warhead. *Cell Chem Biol* **2018**, *25* (1), 78-87.e5. https://doi.org/10.1016/j.chembiol.2017.09.010.

(17) Beck, M.; Schmidt, A.; Malmstroem, J.; Claassen, M.; Ori, A.; Szymborska, A.; Herzog, F.; Rinner, O.; Ellenberg, J.; Aebersold, R. The Quantitative Proteome of a Human Cell Line. *Molecular Systems Biology* **2011**, *7* (1), 549. https://doi.org/10.1038/msb.2011.82.

(18) Liu, X.; Zhang, X.; Lv, D.; Yuan, Y.; Zheng, G.; Zhou, D. Assays and Technologies for Developing Proteolysis Targeting Chimera Degraders. *Future Medicinal Chemistry* **2020**, fmc-2020-0073. https://doi.org/10.4155/fmc-2020-0073.

(19) Zengerle, M.; Chan, K.-H.; Ciulli, A. Selective Small Molecule Induced Degradation of the BET Bromodomain Protein BRD4. *ACS Chem. Biol.* **2015**, *10* (8), 1770–1777. https://doi.org/10.1021/acschembio.5b00216.

(20) Zoppi, V.; Hughes, S. J.; Maniaci, C.; Testa, A.; Gmaschitz, T.; Wieshofer, C.; Koegl, M.; Riching, K. M.; Daniels, D. L.; Spallarossa, A.; Ciulli, A. Iterative Design and Optimization of Initially Inactive Proteolysis Targeting Chimeras (PROTACs) Identify VZ185 as a Potent, Fast, and Selective von Hippel–Lindau (VHL) Based Dual Degrader Probe of BRD9 and BRD7. *J. Med. Chem.* **2019**, *62* (2), 699–726. https://doi.org/10.1021/acs.jmedchem.8b01413.

(21) Smith, B. E.; Wang, S. L.; Jaime-Figueroa, S.; Harbin, A.; Wang, J.; Hamman, B. D.; Crews, C. M. Differential PROTAC Substrate Specificity Dictated by Orientation of Recruited E3 Ligase. *Nat Commun* **2019**, *10* (1), 131. https://doi.org/10.1038/s41467-018-08027-7.

(22) Schwalm, M. P.; Krämer, A.; Dölle, A.; Weckesser, J.; Yu, X.; Jin, J.; Saxena, K.; Knapp, S. Tracking the PROTAC Degradation Pathway in Living Cells Highlights the Importance of Ternary Complex Measurement for PROTAC Optimization. *Cell Chem Biol* **2023**, *30* (7), 753-765.e8. https://doi.org/10.1016/j.chembiol.2023.06.002.

(23) Casement, R.; Bond, A.; Craigon, C.; Ciulli, A. Mechanistic and Structural Features of PROTAC Ternary Complexes. *Methods Mol Biol* **2021**, *2365*, 79–113. https://doi.org/10.1007/978-1-0716-1665-9_5.

(24) Krishnamurthy, V. M.; Estroff, L. A.; Whitesides, G. M. Multivalency in Ligand Design. In *Fragment-based Approaches in Drug Discovery*; Mannhold, R., Kubinyi, H., Folkers, G., Eds.; WILEY-VCH Verlag GmbH & Co.: Weinheim, 2006; Vol. 34, pp 11–53.

(25) Liu, X.; Ciulli, A. Proximity-Based Modalities for Biology and Medicine. *ACS Cent. Sci.* **2023**, *9* (7), 1269–1284. https://doi.org/10.1021/acscentsci.3c00395.

(26) Cao, S.; Kang, S.; Mao, H.; Yao, J.; Gu, L.; Zheng, N. Defining Molecular Glues with a Dual-Nanobody Cannabidiol Sensor. *Nat Commun* **2022**, *13* (1), 815. https://doi.org/10.1038/s41467-022-28507-1.

(27) Raina, K.; Forbes, C. D.; Stronk, R.; Rappi, J. P.; Eastman, K. J.; Gerritz, S. W.; Yu, X.; Li, H.; Bhardwaj, A.; Forgione, M.; Hundt, A.; King, M. P.; Posner, Z. M.; Denny, A.; McGovern, A.; Puleo, D. E.; Garvin, E.; Chenard, R.; Zaware, N.; Mousseau, J. J.; Macaluso, J.; Martin, M.; Bassoli, K.; Jones, K.; Garcia, M.; Howard, K.; Smith, L. M.; Chen, J. M.; Leon, C. A. D.; Hines, J.; Kayser-Bricker, K. J.; Crews, C. M. Regulated Induced Proximity Targeting Chimeras (RIPTACs): A Novel Heterobifunctional Small Molecule Therapeutic Strategy for Killing Cancer Cells Selectively. bioRxiv January 2, 2023, p 2023.01.01.522436. https://doi.org/10.1101/2023.01.01.522436.

(28) Gourisankar, S.; Krokhotin, A.; Ji, W.; Liu, X.; Chang, C.-Y.; Kim, S. H.; Li, Z.; Wenderski, W.; Simanauskaite, J. M.; Yang, H.; Vogel, H.; Zhang, T.; Green, M. R.; Gray, N. S.; Crabtree, G. R. Rewiring Cancer Drivers to Activate Apoptosis. *Nature* **2023**, *620* (7973), 417–425. https://doi.org/10.1038/s41586-023-06348-2.

(29) Mak, S.; Marszal, A.; Matscheko, N.; Rant, U. Kinetic Analysis of Ternary and Binary Binding Modes of the Bispecific Antibody Emicizumab. *mAbs* **2023**, *15* (1), 2149053. https://doi.org/10.1080/19420862.2022.2149053.

(30) Daub, H.; Traxler, L.; Ismajli, F.; Groitl, B.; Itzen, A.; Rant, U. The Trimer to Monomer Transition of Tumor Necrosis Factor-Alpha Is a Dynamic Process That Is Significantly Altered by Therapeutic Antibodies. *Sci Rep* **2020**, *10* (1), 9265. https://doi.org/10.1038/s41598-020-66123-5.

(31) Kast, F.; Schwill, M.; Stüber, J. C.; Pfundstein, S.; Nagy-Davidescu, G.; Rodríguez, J. M. M.; Seehusen, F.; Richter, C. P.; Honegger, A.; Hartmann, K. P.; Weber, T. G.; Kroener, F.; Ernst, P.; Piehler, J.; Plückthun, A. Engineering an Anti-HER2 Biparatopic Antibody with a Multimodal Mechanism of Action. *Nat Commun* **2021**, *12* (1), 3790. https://doi.org/10.1038/s41467-021-23948-6.

(32) Nemoz, C.; Ropars, V.; Frit, P.; Gontier, A.; Drevet, P.; Yu, J.; Guerois, R.; Pitois, A.; Comte, A.; Delteil, C.; Barboule, N.; Legrand, P.; Baconnais, S.; Yin, Y.; Tadi, S.; Barbet-Massin, E.; Berger, I.; Le Cam, E.; Modesti, M.; Rothenberg, E.; Calsou, P.; Charbonnier, J. B. XLF and APLF Bind Ku80 at Two Remote Sites to Ensure DNA Repair by Non-Homologous End Joining. *Nat Struct Mol Biol* **2018**, *25* (10), 971–980. https://doi.org/10.1038/s41594-018-0133-6.

(33) Sijacki, T.; Alcón, P.; Chen, Z. A.; McLaughlin, S. H.; Shakeel, S.; Rappsilber, J.; Passmore, L. A. The DNA-Damage Kinase ATR Activates the FANCD2-FANCI Clamp by Priming It for Ubiquitination. *Nat Struct Mol Biol* **2022**, *29* (9), 881–890. https://doi.org/10.1038/s41594-022-00820-9.

(34) Higuera-Rodriguez, R. A.; Pascali, M. C. D.; Aziz, M.; Sattler, M.; Rant, U.; Kaiser, W. Kinetic FRET Assay to Measure Binding-Induced Conformational Changes of Nucleic Acids. *ACS Sensors*.

(35) Gadd, M. S.; Testa, A.; Lucas, X.; Chan, K.-H.; Chen, W.; Lamont, D. J.; Zengerle, M.; Ciulli, A. Structural Basis of PROTAC Cooperative Recognition for Selective Protein Degradation. *Nat Chem Biol* **2017**, *13* (5), 514–521. https://doi.org/10.1038/nchembio.2329.

(36) Douglass, E. F.; Miller, C. J.; Sparer, G.; Shapiro, H.; Spiegel, D. A. A Comprehensive Mathematical Model for Three-Body Binding Equilibria. *J. Am. Chem. Soc.* **2013**, *135* (16), 6092–6099. https://doi.org/10.1021/ja311795d.

(37) Winter, G. E.; Mayer, A.; Buckley, D. L.; Erb, M. A.; Roderick, J. E.; Vittori, S.; Reyes, J. M.; Di Iulio, J.; Souza, A.; Ott, C. J.; Roberts, J. M.; Zeid, R.; Scott, T. G.; Paulk, J.; Lachance, K.; Olson, C. M.; Dastjerdi, S.; Bauer, S.; Lin, C. Y.; Gray, N. S.; Kelliher, M. A.; Churchman, L. S.; Bradner, J. E. BET Bromodomain Proteins Function as Master Transcription Elongation Factors Independent of CDK9 Recruitment. *Molecular Cell* **2017**, *67* (1), 5-18.e19. https://doi.org/10.1016/j.molcel.2017.06.004.

(38) Werner, M. T.; Wang, H.; Hamagami, N.; Hsu, S. C.; Yano, J. A.; Stonestrom, A. J.; Behera, V.; Zong, Y.; Mackay, J. P.; Blobel, G. A. Comparative Structure-Function Analysis of Bromodomain and Extraterminal Motif (BET) Proteins in a Gene-Complementation System. *Journal of Biological Chemistry* **2020**, *295* (7), 1898–1914. https://doi.org/10.1074/jbc.RA119.010679.

(39) Filippakopoulos, P.; Qi, J.; Picaud, S.; Shen, Y.; Smith, W. B.; Fedorov, O.; Morse, E. M.; Keates, T.; Hickman, T. T.; Felletar, I.; Philpott, M.; Munro, S.; McKeown, M. R.; Wang, Y.; Christie, A. L.; West, N.; Cameron, M. J.; Schwartz, B.; Heightman, T. D.; La Thangue, N.; French, C. A.; Wiest, O.; Kung, A. L.; Knapp, S.; Bradner, J. E. Selective Inhibition of BET Bromodomains. *Nature* **2010**, *468* (7327), 1067–1073. https://doi.org/10.1038/nature09504.

(40) Nicodeme, E.; Jeffrey, K. L.; Schaefer, U.; Beinke, S.; Dewell, S.; Chung, C.; Chandwani, R.; Marazzi, I.; Wilson, P.; Coste, H.; White, J.; Kirilovsky, J.; Rice, C. M.; Lora, J. M.; Prinjha, R. K.; Lee, K.; Tarakhovsky, A. Suppression of Inflammation by a Synthetic Histone Mimic. *Nature* **2010**, *468* (7327), 1119–1123. https://doi.org/10.1038/nature09589.

(41) Anders, L.; Guenther, M. G.; Qi, J.; Fan, Z. P.; Marineau, J. J.; Rahl, P. B.; Lovén, J.; Sigova, A. A.; Smith, W. B.; Lee, T. I.; Bradner, J. E.; Young, R. A. Genome-Wide Localization of Small Molecules. *Nat Biotechnol* **2014**, *32* (1), 92–96. https://doi.org/10.1038/nbt.2776.

(42) Pan, Z.; Zhao, Y.; Wang, X.; Xie, X.; Liu, M.; Zhang, K.; Wang, L.; Bai, D.; Foster, L. J.; Shu, R.; He, G. Targeting Bromodomain-Containing Proteins: Research Advances of Drug Discovery. *Mol Biomed* **2023**, *4* (1), 13. https://doi.org/10.1186/s43556-023-00127-1.

(43) Nowak, R. P.; DeAngelo, S. L.; Buckley, D.; He, Z.; Donovan, K. A.; An, J.; Safaee, N.; Jedrychowski, M. P.; Ponthier, C. M.; Ishoey, M.; Zhang, T.; Mancias, J. D.; Gray, N. S.; Bradner, J. E.; Fischer, E. S. Plasticity in Binding Confers Selectivity in Ligand-Induced Protein Degradation. *Nat Chem Biol* **2018**, *14* (7), 706–714. https://doi.org/10.1038/s41589-018-0055-y.

(44) Hsia, O.; Hinterndorfer, M.; Cowan, A. D.; Iso, K.; Ishida, T.; Sundaramoorthy, R.; Nakasone, M. A.; Imrichova, H.; Schätz, C.; Rukavina, A.; Husnjak, K.; Wegner, M.; Correa-Sáez, A.; Craigon, C.; Casement, R.; Maniaci, C.; Testa, A.; Kaulich, M.; Dikic, I.; Winter, G. E.; Ciulli, A. Targeted Protein Degradation via Intramolecular Bivalent Glues. *Nature* **2024**, 1–8. https://doi.org/10.1038/s41586-024-07089-6.

(45) Wurz, R. P.; Rui, H.; Dellamaggiore, K.; Ghimire-Rijal, S.; Choi, K.; Smither, K.; Amegadzie, A.; Chen, N.; Li, X.; Banerjee, A.; Chen, Q.; Mohl, D.; Vaish, A. Affinity and Cooperativity Modulate Ternary Complex Formation to Drive Targeted Protein Degradation. *Nat Commun* **2023**, *14* (1), 4177. https://doi.org/10.1038/s41467-023-39904-5.

(46) Bauer, K.; Berghoff, A. S.; Preusser, M.; Heller, G.; Zielinski, C. C.; Valent, P.; Grunt, T. W. Degradation of BRD4 - a Promising Treatment Approach Not Only for Hematologic but Also for Solid Cancer. *Am J Cancer Res* **2021**, *11* (2), 530–545.

(47) Nowak, R. P.; Yue, H.; Park, E. Y.; Fischer, E. S. Methods for Quantitative Assessment of Protein Degradation. In *Targeted Protein Degradation*; Cacace, A. M., Hickey, C. M., Békés, M., Eds.; Methods in Molecular Biology; Springer US: New York, NY, 2021; Vol. 2365, pp 247–263. https://doi.org/10.1007/978-1-0716-1665-9_13.

(48) Kim, S. A.; Go, A.; Jo, S.-H.; Park, S. J.; Jeon, Y. U.; Kim, J. E.; Lee, H. K.; Park, C. H.; Lee, C.-O.; Park, S. G.; Kim, P.; Park, B. C.; Cho, S. Y.; Kim, S.; Ha, J. D.; Kim, J.-H.; Hwang, J. Y. A Novel Cereblon Modulator for Targeted Protein Degradation. *Eur J Med Chem* **2019**, *166*, 65–74. https://doi.org/10.1016/j.ejmech.2019.01.023.

(49) Edmondson, S. D.; Yang, B.; Fallan, C. Proteolysis Targeting Chimeras (PROTACs) in "beyond Rule-of-Five" Chemical Space: Recent Progress and Future Challenges. *Bioorg Med Chem Lett* **2019**, *29* (13), 1555–1564. https://doi.org/10.1016/j.bmcl.2019.04.030.

(50) Wu, S.; Jiang, Y.; Hong, Y.; Chu, X.; Zhang, Z.; Tao, Y.; Fan, Z.; Bai, Z.; Li, X.; Chen, Y.; Li, Z.; Ding, X.; Lv, H.; Du, X.; Lim, S. L.; Zhang, Y.; Huang, S.; Lu, J.; Pan, J.; Hu, S. BRD4 PROTAC Degrader ARV-825 Inhibits T-Cell Acute Lymphoblastic Leukemia by Targeting "Undruggable" Myc-Pathway Genes. *Cancer Cell International* **2021**, *21* (1), 230. https://doi.org/10.1186/s12935-021-01908-w.

(51) Zhu, X.; Liu, W.; Tang, X.; Chen, Y.; Ge, X.; Ke, Q.; Liang, X.; Gan, Y.; Zheng, Y.; Zou, M.; Deng, M.; Liu, Y.; Li, D. W.-C.; Gong, L. The BET PROTAC Inhibitor dBET6 Protects against Retinal Degeneration and Inhibits the cGAS-STING in Response to Light Damage. *Journal of Neuroinflammation* **2023**, *20* (1), 119. https://doi.org/10.1186/s12974-023-02804-y.

(52) Xu, L.; Chen, Y.; Mayakonda, A.; Koh, L.; Chong, Y. K.; Buckley, D. L.; Sandanaraj, E.; Lim, S. W.; Lin, R. Y.-T.; Ke, X.-Y.; Huang, M.-L.; Chen, J.; Sun, W.; Wang, L.-Z.; Goh, B. C.; Dinh, H. Q.; Kappei, D.; Winter, G. E.; Ding, L.-W.; Ang, B. T.; Berman, B. P.; Bradner, J. E.; Tang, C.; Koeffler, H. P. Targetable BET Proteins- and E2F1-Dependent Transcriptional Program Maintains the Malignancy of Glioblastoma. *Proceedings of the National Academy of Sciences* **2018**, *115* (22), E5086–E5095. https://doi.org/10.1073/pnas.1712363115.

(53) Chan, K.-H.; Zengerle, M.; Testa, A.; Ciulli, A. Impact of Target Warhead and Linkage Vector on Inducing Protein Degradation: Comparison of Bromodomain and Extra-Terminal (BET) Degraders Derived from Triazolodiazepine (JQ1) and Tetrahydroquinoline (I-BET726) BET Inhibitor Scaffolds. *J Med Chem* **2018**, *61* (2), 504–513. https://doi.org/10.1021/acs.jmedchem.6b01912.